

Department of Environment Systems
Graduate School of Frontier Sciences
The University of Tokyo

2019

Master's Thesis

**Continuous solvothermal synthesis of cobalt
oxide nanoparticle using a high temperature high
pressure water-ethanol mixed solvent**

Submitted February 25, 2020

Adviser: Professor Oshima Yoshito

劉 源

Liu Yuan

Chapter 1	4
1.1 The basis of nanoparticles	4
1.2 Synthesis methods for nanoparticles	4
1.3 High temperature/high pressure hydrothermal synthesis	5
1.3.1 Hydrothermal synthesis	5
1.3.2 Crystal formation	6
1.3.3 Features of high temperature/high pressure hydrothermal synthesis	7
1.3.4 Physical property of high temperature/high pressure water	8
1.3.5 Previous research about mix condition	9
1.4 High temperature/high pressure solvothermal synthesis using ethanol	10
1.5 High temperature/high pressure solvothermal synthesis using water-ethanol mixed solvent .	12
1.5.1 Physical property of high temperature/high pressure water-ethanol mixed solvent	13
1.5.2 NPs synthesis using high temperature/high pressure water-ethanol mixed solvent	14
1.6 Objective	15
1.6.1 Objective	15
1.6.2 Target material	15
1.6.3 Items in discussion	16
1.7 Summary	17
Chapter 2	25
2.1 Materials	25
2.2 Apparatus and procedure	25
2.3 Reactor design	26
2.4 Analysis method	27
2.4.1 XRD	27
2.4.2 TEM	28
2.4.3 UV-Vis	29
2.5 Summary of this chapter	30
Chapter 3	36
3.1 Co ions conversion	36
3.1.1 Nanoparticle formation	36
3.1.2 Conversion	38
3.2 Lower ethanol ratio range	40

3.2.1 Classical crystal growth theory	40
3.2.2 Nanoparticle size	43
3.2.2 Nanoparticle shape.....	45
3.3 Higher ethanol ratio range.....	48
3.3.1 Valance number change of cobalt oxide nanoparticles	48
3.3.2 Reaction time change at 0.6 molar ratio of ethanol condition.....	49
3.4 Summary of this chapter	50
Chapter 4 Conclusion.....	76
Reference	77
Acknowledgments	80

Chapter 1

1.1 The basis of nanoparticles

Nanoparticles are particles having a diameter of about 1 to 100 nm. The particles in this region change greatly in the properties of the substance, and exhibit different properties from the bulk [1]. For example, it has been reported that the proportion of atoms present on the particle surface increases and the surface effect appears remarkably [2], and the quantum size effect that changes the band gap energy appears when electrons are confined in that region. Industrially, nanoparticles such as silica, nickel, titanium dioxide, alumina, zinc oxide, and iron oxide are used as fillers, cosmetics, pigments, and the like on a scale of 100 ton / year or more [3]. In addition, attempts are being made to utilize various inorganic nanoparticles for the use of catalysts, optical materials, electrodes, and the like, and a wide variety of synthesis techniques are being studied.

When these inorganic nanoparticles are used as a raw material, control of particle size, distribution, crystal structure, composition, dispersibility, and the like is indispensable. It is thought that not only the search for new materials, but also the development of new functions and the enhancement of efficiency and function, the reduction in size and thickness, and the saving of resources through nanostructure control will lead to the development of nanotechnology.

1.2 Synthesis methods for nanoparticles

Particle synthesis methods can be broadly classified into a top-down method, in which raw materials are pulverized into particles, and a bottom-up method, in which particles are precipitated from precursors such as ions and molecules (Figure 1-1). The top-down method is characterized in that particles having good crystallinity can be synthesized in a large amount because the synthesis is performed in a solid phase. However, it is difficult to control nanoparticles of 100 nm or less, and the bottom-up method is mainly used for the synthesis of nanoparticles. This bottom-up method can be further classified into a gas phase method and a liquid phase method. In general, when the gas phase method is used, the reaction is performed at a high temperature and the crystallinity is high, and single nano (particles with a diameter of 10 nm or less) can be synthesized. Have difficulty. On the other hand, when the liquid phase method is used, the operability of the form and size is high due to the

effect of the solvent, but the crystallinity is low. At present, many studies have been made on the synthesis of composite oxides that combine not only a single metal species but also a plurality of metal species, and are expected to be applied to functional materials. The synthesis of this composite oxide is characterized in that the degree of freedom of the crystal structure is increased as compared with a single metal oxide. As a conventional synthesis method, a method in which a single component carbonate or oxide is used as a starting material to synthesize by a solid-phase reaction is generally used. (> 1000 ° C) and long-time (hour-days) treatment, it has been difficult to control the crystal in nano order. For such a complex oxide system, a new nanoparticle synthesis technology is desired in order to control the nanostructure more highly.

In this study, we focused on supercritical fluids, which are expected to be used as a new nanoparticle synthesis technology in recent years. In the following, the outline of supercritical hydrothermal synthesis is described, followed by the features of supercritical water and trends in supercritical hydrothermal synthesis up to now.

1.3 High temperature/high pressure hydrothermal synthesis

1.3.1 Hydrothermal synthesis

First, the hydrothermal reaction will be described. The hydrothermal synthesis method is a method of obtaining an oxide product by dissolving and precipitating a raw material in hot water under pressure, and is currently in practical use in many processes. In the hydrothermal reaction, after a hydroxide is produced by hydrolysis of the raw material (Eq. 1-1), the hydroxide is dehydrated and condensed to produce a target metal oxide (Eq. 1-2).



Pressurization enables synthesis in a temperature range exceeding the boiling point under normal pressure. By utilizing such a change in the physical properties of the solvent, the solubility and reaction rate of the raw materials can be controlled, and thus it is considered to be a useful synthesis method for metal oxides.

1.3.2 Crystal formation

Crystal formation occurs in both the gas phase and the liquid phase. Here, the mechanism of crystal formation in the liquid phase will be described. In the process of generating particles by the bottom-up method, a process in which elements constituting particles such as atoms and molecules gather to form a very small solid, that is, an initial nucleus, is called a nucleation process. In classical nucleation theory, the free energy change ΔG associated with the formation of the initial nucleus in homogeneous nucleation is expressed as the sum of the cohesive energy of the constituent elements and the interface energy of the initial nucleus as shown in the following equation (Eq. 1-3) [4]. This free energy change depends on the initial nuclear radius as shown in Fig. 1-2. When the degree of supersaturation is $S > 1$, it has a maximum value ΔG^* at $r = r^*$, and the energy barrier for uniform nucleation is Become.

$$\Delta G = -\frac{4kT \ln S}{3v_1} r^3 + 4\pi\sigma r^2 \quad (\text{Eq. 1-3})$$

k: Boltzmann's constant, T: absolute temperature, S: supersaturation, v_1 : volume occupying one component in a particle, σ : surface energy, r: radius of initial nucleus

When particles are precipitated from a solution, atoms and molecules constituting elements of the initial nucleus repeatedly undergo aggregation and dissolution. When the radius of the initial nucleus formed by the aggregation is larger than r^* , the free energy of the system becomes more stable as the initial nucleus becomes larger. That is, initial nucleus growth follows. On the other hand, if an initial nucleus smaller than r^* is formed, the initial nucleus will dissolve and return to atoms and molecules to be more energetically stable. Therefore, this r^* is an index for judging the stability of the formed initial nucleus, which is called a critical nucleus radius. The critical nucleus radius gives the minimum standard of the particle radius that can be generated. However, as can be seen from r^* in Fig. 1-2, if the supersaturation is increased and the interface energy is decreased, the critical nucleus radius becomes smaller. That is, when synthesizing nanoparticles having a small size, these points should be considered.

The supersaturation is a value obtained by dividing the concentration C of the particle component present in the solution by the saturation solubility C_0 , and when the supersaturation is larger than 1,

particles are generated. To achieve a large degree of supersaturation and synthesize small nanoparticles, C or C_0 may be controlled. On the other hand, the interfacial energy is determined by the combination of the solvent and the nanoparticles used, but can also be controlled by adsorbing the third component on the surface, similarly to the surface energy of general solids.

In the case of producing nanoparticles by dissolving molecules dissolved in a solvent, the concentration C of the particle component can be increased by using a solvent having high solubility and temperature and pressure conditions. From this point, if C_0 can be reduced to the opposite condition, the supersaturation degree can be further increased. In the case where nanoparticles are generated by a chemical reaction, if the reaction rate is sufficiently higher than the particle generation rate, C increases. As described above, it is possible to design a reaction operation for synthesizing nanoparticles from the viewpoint of free energy, but in addition to this, the viewpoint of suppressing nuclear growth is also important.

In the actual particle synthesis process, in parallel with the nucleation, nucleus growth in which the particle components existing in the solvent precipitate on the existing initial nuclei proceeds. In order to synthesize smaller nanoparticles, it is necessary to suppress this nucleus growth. Here, let us consider a case where the particle component is gradually supplied and a case where the particle component is rapidly supplied under the condition that the saturated solubility C_0 is constant (Fig. 1-3). If the particle component is supplied gradually, the supplied particle component is consumed for the formation of the initial nucleus and used for the growth of the already existing initial nucleus. On the other hand, when the particle components are supplied rapidly, there is no initial nucleus at that time, and most of the initial nucleus is consumed for initial nucleus growth, and as a result, particle growth is suppressed.

As described above, the approach to nanoparticle synthesis was discussed from the viewpoint of free energy and speed. One of the solvents that can realize a suitable synthesis environment is a supercritical fluid.

1.3.3 Features of high temperature/high pressure hydrothermal synthesis

In this section, the features of particle synthesis using supercritical water will be described. Supercritical water has a very low dielectric constant compared to normal-temperature and normal-

pressure water, so the hydrothermal reaction proceeds rapidly and the solubility of inorganic substances becomes extremely low. Production is promoted, and small nanoparticles can be produced. In addition, since the viscosity is low, rapid mixing is possible, and the growth of particles is suppressed. From this, it is considered that supercritical water is suitable as a nanoparticle synthesis field. The physical properties of supercritical water, which is important in supercritical hydrothermal synthesis, are described below.

1.3.4 Physical property of high temperature/high pressure water

Here, changes in physical properties of water that are important in supercritical hydrothermal synthesis are described. Supercritical water refers to water above the critical point (373.9 ° C, 22.1 MPa). Further, by applying a pressure higher than the saturated vapor pressure, the water can be used as a solvent in a high-temperature region. Furthermore, when the pressure exceeds the critical pressure, no matter how much the temperature is changed, a phase change such as evaporation or condensation does not occur, and the physical property value is continuously changed.

Table 1-1 shows the transport properties of supercritical water, gas and liquid. It can be seen that the transport properties of supercritical flowing water are intermediate between liquid and gas. That is, while the supercritical fluid has a density comparable to that of a liquid, the kinematic viscosity, the diffusion coefficient, and the like show relatively small values close to those of a gas. As mentioned in section 1.2, it has almost the properties of gas and liquid, so it can be said that it is close to "dense water vapor".

Figure 1-4 shows the temperature dependence of the physical properties of water at a pressure of 25 MPa. Near the critical point, small changes in temperature or pressure have been shown to cause a rapid change in dielectric constant. In the calculation of the relative permittivity, the following equation expressed as a function of the density ρ and the temperature T is used in the Uematsu-Franck model [5]. $A_i (i = 1 - 10)$ is a constant value, $\rho^* = \rho / \rho_0$, $T^* = T / T_0$ ($\rho_0 = 1000 \text{ kg} / 10^3$, $T_0 = 298.15 \text{ K}$).

$$\varepsilon = 1 + \left(\frac{A_1}{T}\right)\rho + \left(\frac{A_2}{T} + A_3 + A_4T^*\right)\rho + \left(\frac{A_5}{T} + A_6T + A_7T\right)\rho^{*3} \quad (\text{Eq. 1-4})$$

$$+ \left(\frac{A_8}{T^{*2}} + \frac{A_9}{T^*} + A_{10}\right)\rho^{*4}$$

As can be seen from Fig. 1-4, the relative permittivity of water is about 80 at room temperature, but the relative permittivity decreases with increasing temperature, and takes a very low value above the critical point (for example, 400 ° C.). The dielectric constant is 5.9 at C and 30 MPa. As a result, while the inorganic substance has a high solubility up to around 300 ° C. used for hydrothermal synthesis, the solubility of the inorganic substance is greatly reduced in a supercritical state. The Born equation (Eq. 5), which represents the solvation energy, is shown in the following equation. It can be seen that the solvation energy decreases as the relative permittivity of the solvent decreases [6].

$$\Delta_{solv}G = -\left(\frac{z_i^2 e^2 N_A}{8\pi\epsilon_0 r_i}\right)\left(1 - \frac{1}{\epsilon_{H_2O}}\right) \quad (\text{Eq. 1-5})$$

z_i: valance number of ion, r_i: radius of ion

And the dissolution equilibrium constant is given by Eq. 1-6 [7].

$$\ln K(T, \varepsilon) = \ln(T_0, \varepsilon_0) - \frac{\Delta H}{R}\left(\frac{1}{T} - \frac{1}{T_0}\right) - \frac{c}{RT}\left(\frac{1}{\varepsilon} - \frac{1}{\varepsilon_0}\right) \quad (\text{Eq. 1-6})$$

$$+ \frac{\theta}{R}\left(\frac{1}{T} - \frac{1}{T_0}\right)$$

K: Equilibrium constant, T: Temperature, ε: Dielectric constant, ΔH: Reaction enthalpy, R: Gas constant, c: Constant determined by the difference in polarity between the original system and the generated system, θ: Non-electrostatic effect

Thus, in addition to the reaction enthalpy, an electrostatic solvent effect due to a change in the dielectric constant of the solvent and a non-electrostatic effect such as rearrangement of the solvent are considered.

1.3.5 Previous research about mix condition

The most significant feature of supercritical hydrothermal synthesis is that the reaction field can be changed quickly and high supersaturation conditions can be realized by taking advantage of the

characteristics of supercritical water described in section 1.3.4. It is important that the rate of change of the reaction field, here the rate of temperature rise, is sufficiently large relative to the rate of the conventional hydrothermal reaction. For this reason, in supercritical hydrothermal synthesis, rapid mixing and rapid temperature increase using a flow-type reactor have been considered important.

In the flow-type reaction apparatus, the size of the flow path is important for mixing the fluid. The relationship between the average particle size of the synthesized oxide nanoparticles and the Reynolds number (Re) in the flow channel has been reported when the inner diameter and flow rate of the mixing section and the pipe connected immediately after mixing are changed [8] (Figure 1-5). Although the average particle size differs depending on the metal species, the average particle size decreases with increasing Re number from the laminar flow region to the turbulent flow region, and the average particle size becomes almost constant on the high Re side of 4×10^4 or more. This indicates that by setting the Re number in the mixing section and immediately after the pipe to 4×10^4 or more, it is possible to set a reaction rate-limiting condition that is not affected by the mixing process. This is important not only to obtain homogeneous oxide nanoparticles, but also to accurately analyze the reaction (particle generation) mechanism. The condition of Re is at least one order of magnitude larger than the critical Reynolds number when transitioning from laminar to turbulent. This indicates that even in a turbulent field, a transition region occurs until the flow state is homogenized, which affects the particle size and distribution of the synthesized particles.

1.4 High temperature/high pressure solvothermal synthesis using ethanol

Nearcritical and supercritical fluids (NCFs and SCFs) have been developed as environmentally benign solvents, characterized primarily by continuously adjustable physicochemical properties (for example density, viscosity, and dielectric constant, etc.) with temperature and pressure [9, 10]. For the past two decades, the properties of near- and supercritical fluids have been a growing research area motivated by a variety of promising applications, such as chemical syntheses [11], extractions and separations [12], material processing [13], and waste detoxification [14]. SCFs possess a wide range of gas-like to liquid-like properties and can be employed as unique media to overcome poor solvent strength of gases and hindered mass transportation in conventional liquids. Moreover, their inherently high tunability opens up additional opportunities to tailor the reactions (phase behavior [15],

equilibrium [16, 17], reaction rate [18], and selectivity [19, 20]) coupled with facile separation and recovery by simply manipulating temperature, pressure, or cosolvent concentration. In contrast, NCFs provide more accessible pressure and temperature than those of SCFs, and liquid-like properties and dissolving power with considerable tunability, while maintaining many of the same separation advantages of SCFs.

Non-associating fluids (such as carbon dioxide, fluoroform, and ethane) have moderate critical temperatures, but they display limited dissolving power for compounds of no or little volatility without the addition of cosolvent. On the contrary, associating fluids (such as water, alcohols, and acetic acid) have much higher critical temperatures, but they are capable of solvating a wide range of heavy compounds under near- or supercritical conditions. To date, supercritical (SC) carbon dioxide ($T_c = 31.1\text{ }^\circ\text{C}$, $P_c = 7.38\text{ MPa}$) and water ($T_c = 374\text{ }^\circ\text{C}$, $P_c = 22.1\text{ MPa}$) have been the focus of research efforts and industrial applications towards benign and tunable solvents. Cosolvents such as alcohols are frequently added to SC CO₂ to enhance the solubility of non-volatile compounds, which may change the critical properties and complicate the phase behavior. On the other hand, the high temperature and pressure of supercritical water (SCW) challenges the material and operation. More importantly, it eliminates most chemical syntheses other than oxidation due to the decomposition promoted by high temperature. In comparison with SCW, ethanol has more accessible critical properties ($T_c = 241\text{ }^\circ\text{C}$, $P_c = 6.14\text{ MPa}$), and is less corrosive and more reactive. One can also expect a pronounced enhancement of solubility in SC ethanol compared with that in CO₂ due to the hydrogen-bonding ability of the former. More investigations have been performed in hot methanol which, however, cannot be considered a benign solvent because of its toxicity, especially in pharmaceutical and food processing. Several reactions of industrial significance have been successfully presented in hot ethanol up to its critical temperature, for example, catalytic etherification from tertiary alcohol [21], alkylation of toluene to produce p-ethyltoluene [22], and hydrogen-transfer reductions of aldehydes and ketones without catalysts [14]. Still our fundamental understanding for NC and SC ethanol is very limited. In addition, SC ethanol could provide an experimentally more accessible analog of SCW.

The characterization of SCFs has been pursued extensively using experimental [23] and theoretical [24] approaches in the last two decades. Various in situ spectroscopic techniques (UV-VIS,

fluorescence, FT-IR, NMR, etc.) have proven to be powerful probes for SCF solution chemistry [25]. Kamlet–Taft solvent parameters π^* , α , and β are one of the important approaches in achieving insight into solvent strength for pure SCFs and mixtures [26]. The parameters π^* , α and β are indexes for dipolarity/polarizability, hydrogen-bond donating acidity, and hydrogen-bond accepting basicity, respectively [27]. The experimental measurements of π^* , α , and β are based on the solvent-induced solvatochromic shift of certain spectroscopic indicators. Solvatochromism is defined as the phenomenon that UV–VIS absorption spectra of some molecules are highly sensitive to the surrounding medium, and the position of maximum absorption is believed to be indicative of certain solvent property, such as polarity or hydrogen-bonding. The π^* , α , and β values for more than 200 traditional solvents have been measured and compiled [28].

The solvent parameters π^* , α , and β are used with linear solvation energy relationship (LSER) to correlate a variety of configurational properties in solution: solubility, partition coefficient, thermodynamic and kinetic properties of chemical reaction, etc. including those under extreme conditions [29]. A simplified LSER theory can be expressed as follows:

$$XYZ = (XYZ)_0 + s\pi^* + a\alpha + b\beta \quad (\text{Eq. 1-6})$$

where XYZ and $(XYZ)_0$ denote the solvent-dependent physicochemical properties in a given solvent and in a reference solvent (gas or inert solvent); s , a , and b are solvent-independent coefficients denoting the susceptibility of the property to the applied parameters. The multiparameter approach serves as a good approximation of solvent effects, which takes into account three aspects of solvation: non-specific polar interactions as well as hydrogen-bond donating and accepting interactions.

1.5 High temperature/high pressure solvothermal synthesis using water-ethanol mixed solvent

In this research, before we start to the nanoparticle synthesis process in the high temperature and high pressure water-ethanol mixed solvent, firstly we need to study the basic physic property data of water-ethanol mixed solvent at high temperature and high pressure condition, and the property change of water-ethanol mixed along with the water/ethanol ratio change at high temperature and high pressure condition.

1.5.1 Physical property of high temperature/high pressure water-ethanol mixed solvent

Alcohol-water mixtures are important for many fields ranging from fundamental science to industrial applications [30], which can be attributable to their solution features [31] and macroscopic properties [32]. The hydrogen bond is one of the most prevalent intermolecular interactions, and the relationship between microscopic and macroscopic properties for alcohol-water mixtures has been investigated from fundamental physical properties [33], spectroscopic experiments [34] and computer simulations [35]. It has been pointed out that the hydrogen bonds remain at supercritical conditions [36] and bring about unique properties different from those of ambient conditions at high temperatures and high pressures [37]. Safarov et al. [38] measured densities of methanol-water, ethanol-water and n-propanol-water mixtures at temperatures up to 573 K and at pressures up to 60 MPa in $x_a = 0.25$ increments. Xiao et al. [39] have measured densities of methanol-water mixtures at temperatures between 323 K and 573 K and pressures of 7.0 MPa and 13.5 MPa. Bulemela et al. [40] reported on densities of methanol-water mixtures at 573 and 588 K and at pressures in the 10e20 MPa range. In particular, Xiao et al. [41] and Bulemela et al. [42] have discussed the alcohol composition dependence of the density in detail and showed that the excess molar volumes calculated from the measured densities increase from negative to positive with increasing alcohol composition around the critical temperature of the alcohol. These results show the importance of composition dependence of physical properties of alcohol-water mixture at high temperatures and high pressures. On the other hand, there are few reports of alcohol-water mixture viscosities above 373 K considering the interesting features of their composition dependence [43].

Based on the previous research about basic physic property of water-ethanol mixed solvent above, we used the density and viscosity data of water-ethanol mixed solvent at different water/ethanol ratio and high temperature and high pressure from the research about measurement and correlation of density and viscosity of n-alcohol-water mixtures at temperatures up to 618 K and at pressures up to 40 MPa by Takumi et, al. In this study, density and viscosity of alcohol-water mixtures at temperatures from 523.2 to 618.2 K and at pressures up to 40 MPa are measured to elucidate the volumetric and viscometric behavior. At these conditions, the extent of hydrogen bonding of water and alcohol characterized by the proton NMR chemical shift change dramatically [44], and a large change of the physical properties corresponding to changes in hydrogen bonding can be expected. Viscosities were

correlated with the Eyring's theory and Peng-Robinson EoS. In addition, a volume translated equation of state [45] was adopted to determine the densities. And data of density and viscosity dependence and critical loci of water-ethanol mixed solvent are shown in the Fig.1-6, Fig. 1-7.

1.5.2 NPs synthesis using high temperature/high pressure water-ethanol mixed solvent

Continuous hydrothermal synthesis of metal oxide nanoparticles (NPs) using supercritical water has been widely researched as an environmentally benign method for producing high-crystalline functional metal oxide NPs. With the drastic decrease of water density and permittivity along with temperature and pressure increase of water to supercritical state (374°C, 22.1MPa), solubility of metal oxides sharply decreases, which result in NPs formation resulted from the high degree supersaturation. Besides hydrothermal synthesis using supercritical water, supercritical ethanol is also a kind of widely utilized solvent for solvothermal synthesis of NPs [46]. Compared with water, ethanol has a lower critical temperature and pressure (241°C, 6.14MPa), which provide a benign condition for NPs synthesis. It is reported that ethanol can also work not only as solvent, but as surface modifier at the synthesis process of NPs [47]. Furthermore, because of the reduction environment compared with water, besides metal oxide nanoparticles, metal nanoparticles are synthesized in supercritical ethanol [48]. Based on the characteristics of supercritical ethanol mentioned above, it becomes possible to change the critical point, acid/base property, and even oxidation/reduction property of the high temperature and high pressure water-ethanol mixture solvent by only changing the water-ethanol ratio of the solvent. It is reported that barium titanate nanoparticles are synthesized with the crystallinity of 90% [49] and that the crystallization of yttrium aluminum garnet nanoparticles are promoted by the mix of ethanol into water [50]. Also the crystallinity or the size [51] of NPs could be changed by the mixture solvent. There is little research focusing on the oxidation/reduction property changes in water-ethanol mixture, which may cause changes on the composition of synthesized nanoparticles. Also the mechanism of how the changes of property of mixed solvent at water-ethanol ratio affect the synthesis of NPs, also need to be confirmed.

1.6 Objective

1.6.1 Objective

So far we talked about the broad prospects of nanoparticles and some traditional synthesis methods of them. And supercritical water as a solvent has a low permittivity and high diffusion coefficient near its critical temperature and pressure, thus supercritical hydrothermal synthesis as a method to synthesize nanoparticles has been studied for a long time and utilized widely. On the other hand, ethanol has a lower critical temperature and pressure (241°C, 6.14MPa), which provide a benign condition for NPs synthesis. And it is reported that ethanol can also work not only as solvent, but as surface modifier at the synthesis process of NPs. Furthermore, because of the reduction environment compared with water, besides metal oxide nanoparticles, metal nanoparticles are synthesized in supercritical ethanol. So based on the characteristics of supercritical ethanol mentioned above, it becomes possible to change the critical point, acid/base property, and even oxidation/reduction property of the high temperature and high pressure water-ethanol mixture solvent by only changing the water-ethanol ratio of the solvent. While there is little research focusing on the oxidation/reduction property changes in water-ethanol mixture, which may cause changes on the composition of synthesized nanoparticles. Also the mechanism of how the changes of property of mixed solvent at water-ethanol ratio affect the synthesis of NPs, also need to be confirmed.

So the purpose of this research is to elucidate the effect of mixing ethanol into water on the synthesis of metal nanoparticles at high temperature and high pressure condition.

1.6.2 Target material

Synthesis of cobalt oxide NPs was selected as a model reaction. Cobalt oxides have a wide range of applications as supported catalysts for the Fischer–Tropsch process, supercapacitor electrodes, anodes for Li-ion batteries, water oxidation catalysts, magnetic materials, and in biomedicine. The phase, crystallite size, size distribution, crystallinity faceting, and specific surface area of these materials at the nanometer scale are strongly correlated to their fundamental properties and their potential applications. For example, as a Fischer–Tropsch catalyst, cobalt oxide particles <10 nm have better turnover and lower reduction temperatures than larger particles¹² (>20 nm) as well as improved catalytic activity. Similarly, the surface area of an electrode of a supercapacitor greatly influences its

performance.¹⁴ Therefore, there is a significant amount of interest in the ability to control the particle size of cobalt oxides below 10 nm, in a scalable manufacturing process.

The synthesis routes for cobalt oxides nanoparticles such as CoO and Co₃O₄ include solid state synthesis, soft chemistry, gas phase synthesis, thermal decomposition and hydrothermal synthesis. Some of the aforementioned synthesis methods are not able to consistently deliver small size nanoparticles with a narrow size distribution using a process that is readily scalable. For example, a synthesis method yielding very small (≥ 3.5 nm) cobalt oxide nanoparticles was developed by Xu and Zeng, but it is time consuming (>72 h) and requires the use of surfactants. Consequently, there is a need to develop green, rapid, inexpensive, and scalable routes for the synthesis of small cobalt oxide nanoparticles

1.6.3 Items in discussion

In this research, to elucidate the effect of mixing ethanol into water on the synthesis of metal nanoparticles at high temperature and high pressure condition, two aspects of nanoparticles synthesis will be put into discussion.

Firstly, the physical property changes along with the water/ethanol ratio of the mixed solvent change are the key point at this research. Experiments at different water/ethanol ratio but the same temperature and pressure condition will be conducted, and the size, shape, composition, and valence number of produced cobalt nanoparticles will be measured. And how the changes of the size, shape, composition, and valence number of produced cobalt nanoparticles can be related to the physical property changes along with the water/ethanol ratio of the mixed solvent change will be discussed.

Then, to study the cobalt nanoparticles synthesis process specifically, experiments at different reaction time at each water/ethanol ratio of the mixed solvent will also be conducted, and the size, shape, composition, and valence number of produced cobalt nanoparticles will be measured. And how the changes of the size, shape, composition, and valence number of produced cobalt nanoparticles can be dependent to the reaction time change will be discussed.

1.7 Summary

In this paper, after describing the background of the research in this chapter, the experimental and analytical methods are described in Chapter 2. After that, the experiment results will be discussed in chapter 3. Finally, in chapter 4, I will summarize and make a conclusion for this research.

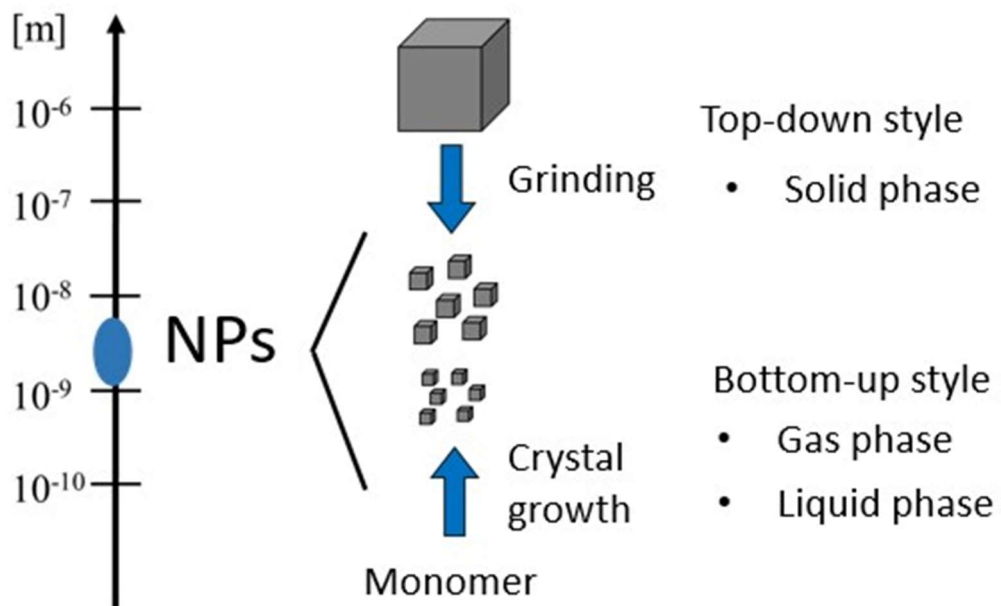


Fig. 1-1. Synthesis method of metal oxide particles

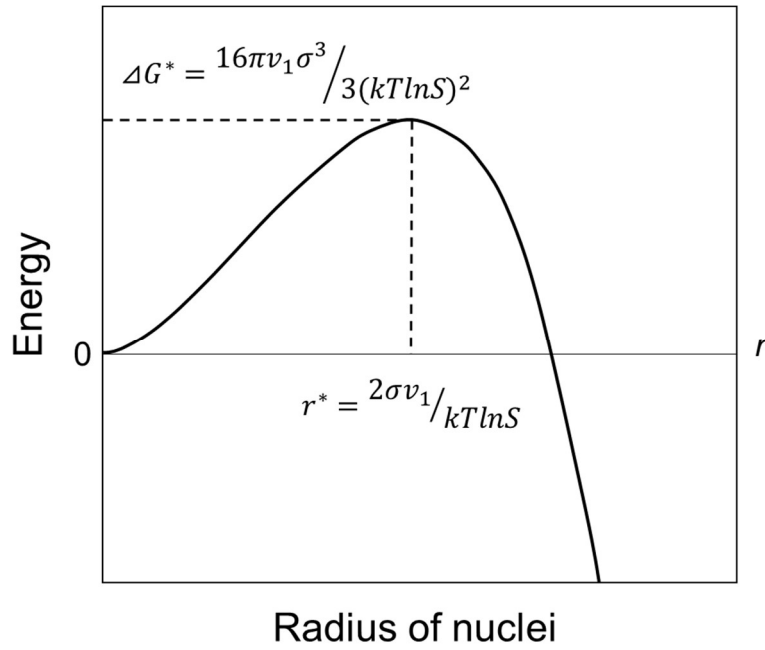


Fig. 1-2. Relationship between initial nuclear radius and free energy change in homogeneous nucleation

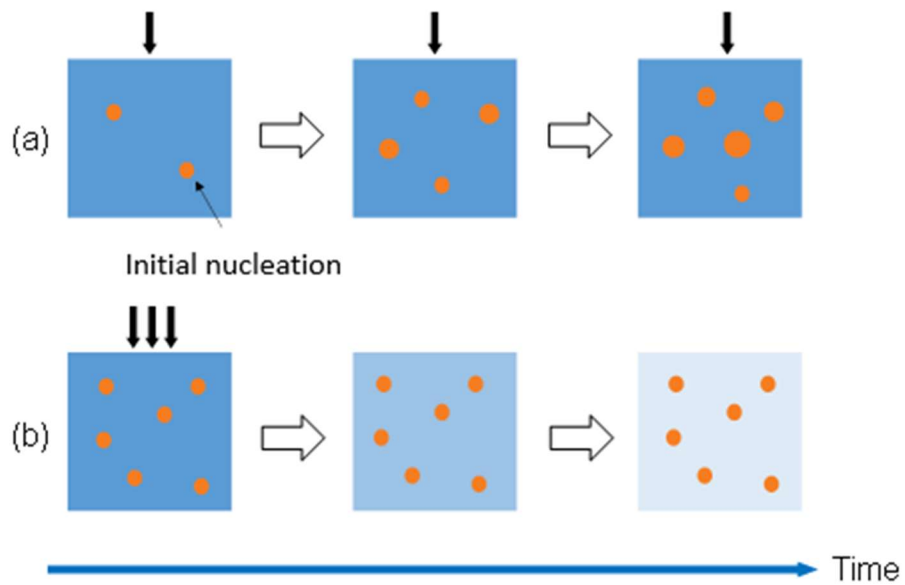


Fig. 1-3. (a) When the particle component is supplied gradually; (b) When particle components are supplied at once, Schematic diagram of initial nucleus growth and growth process

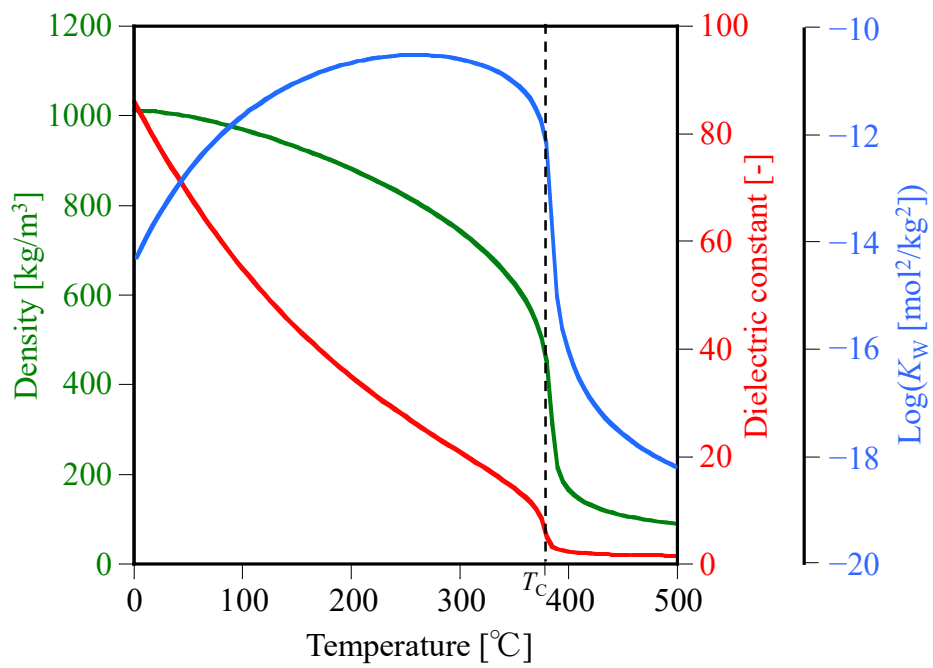


Fig. 1-4. Temperature dependence of water properties at 25 MPa

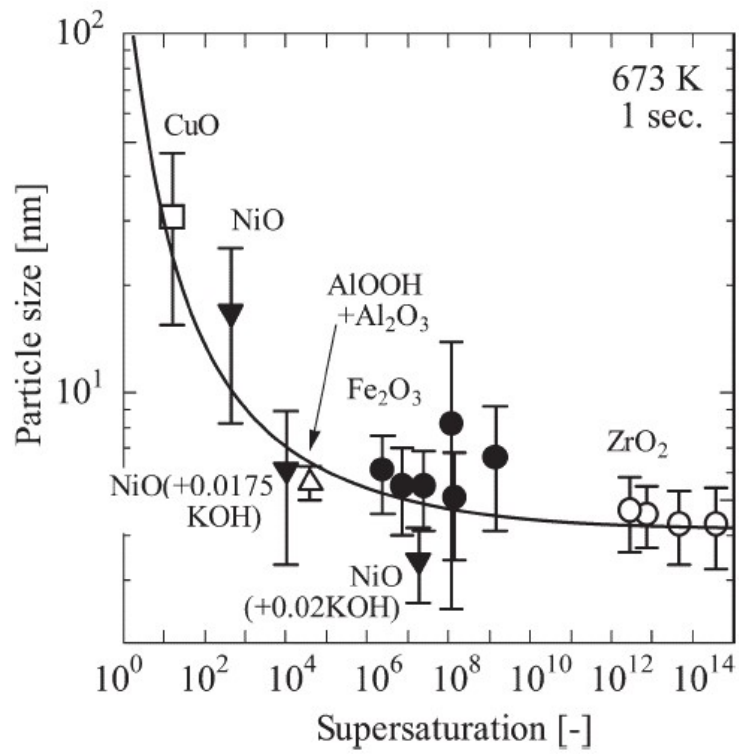


Fig. 1-5. Relationship between average particle size of synthesized oxide nanoparticles and Reynolds number (Re) in channel [8]

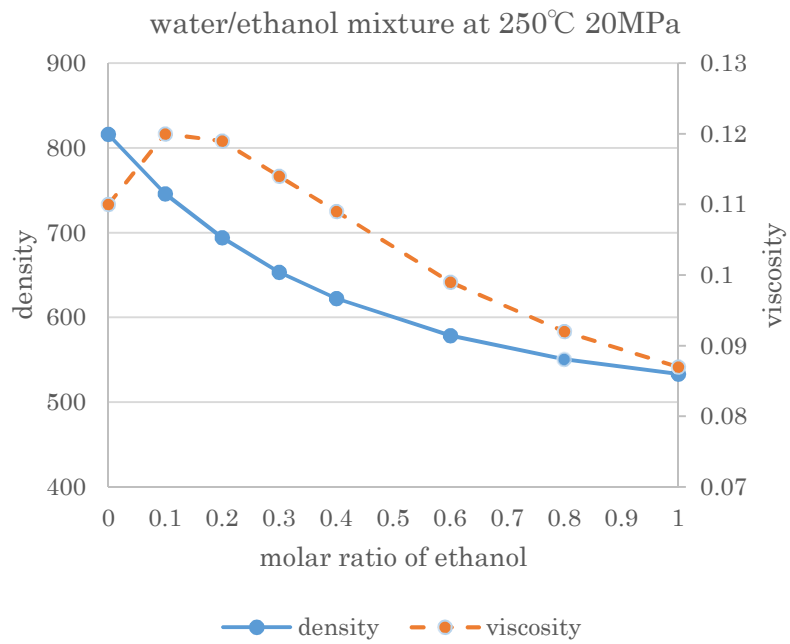


Fig. 1-6. Density and viscosity change along with the molar ratio of ethanol at 250°C 20MPa.

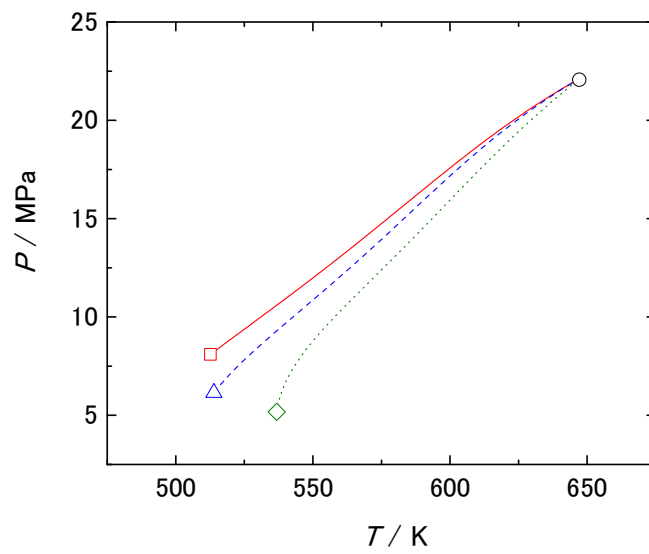


Fig. 1-7. Critical loci for methanol, ethanol and n-propanol-water mixtures calculated by the Peng-Robinson EoS and Heidemann and Khalil method. Solid, dashed and dot lines represent methanol-water, ethanol-water and n-propanol-water mixtures. Circle, square, triangle and diamond represent the critical point of water, methanol, ethanol and n-propanol. [54]

Chapter 2

2.1 Materials

In the experiment, used reagents are as following.

Distilled water (purified by AQUARIUS (made by RFD240HA, ADVANTEC))

Co(NO₃)₂ Wako

HNO₃ Wako

Ethanol 99.5% Wako

In the analysis, used materials are as following.

Co standard solution Wako

2.2 Apparatus and procedure

In this study, supercritical hydrothermal synthesis was performed using the flow reactor shown in Fig. 2-1. The water and ethanol heated in advance by the electric furnace and the respective adjustment solutions were rapidly mixed so as to be in a high temperature high pressure state. For the mixing part, a swirl mixer made by SUS316 was utilized. The diameter of the main line of this swirl mixer is 0.8 mm, and diameter of the subline of this swirl mixer is 0.5 mm. It has been reported that when the Re of the mixing part is 4×10^4 or more, the reaction is not limited to diffusion but limited to reaction [8]. And in this research, it is almost satisfied at 250 °C, 20 MPa for water-ethanol mixed solvent. In this process, water-ethanol mixture was heated by the oven and then fed into the swirl mixer from line 2 and 3. The cobalt precursor Co(NO₃)₂ aqueous solution was also pumped into the mixer from line 1 simultaneously. And with line 1 of 10 g/min, line 2 of 20 g/min, line 3 of 20 g/min, totally 50 g/min stream flow through the mixing part. The raw metal salt aqueous solution was cooled to just before mixing in order to rapidly raise the temperature. The residence time was manipulated by changing the volume of the reaction tube so as to achieve a predetermined residence time. The water/ethanol ratio of the mixed solvent is controlled to ranging from 1/0~0.2/0.8 by changing the flow rate of influent 2, 3, and 4, 5. The specific flow rate of each influent at each water/ethanol molar ratio is listed at Table.2-1. After the reaction, internal cooling water was introduced at 30 mL/min to enable rapid cooling. The

pressure was controlled by applying a constant pressure with a back pressure valve (BP66-112865, Go Inc.). The temperature and pressure in each reaction section were output to a data logger (SMARTDAC + GM, Yokogawa) and monitored. The recovered nanoparticle suspension was subjected to pressure filtration with nitrogen gas using a nitrocellulose filter (Merck Millipore, VSWPI14250, diameter 142 nm, pore size 0.1 μm). After filtration, the nitrocellulose filter was transferred to a vacuum dryer (Yamato, ADP-31), dried for 24 hours, and collected.

About the operates in the experiment process, before turning on the water and ethanol feeding pump, the faucets of cooling water are opened. Then the working condition of each pump need to be checked. After the pumps turned on, water is feed at the very first moment. The pressure of inside the reactor is adjusted to 20 MPa by manipulating the back pressure valve. Then the ovens are turned on and temperature are set to 450 $^{\circ}\text{C}$. When the temperature monitoring of the water-ethanol mixed solvent immediately before the internal cooling water increased to 200 $^{\circ}\text{C}$, switch influent 2 and 4 from water to feeding ethanol, and adjust the pump rate to calculated value according to the water/ethanol molar ratio desired. Once the temperature stabilized to 250 $^{\circ}\text{C}$, switch the influent 1 from water to cobalt precursor solution at flow rate of 10 mL/min. When the effluent start to get turbid, the effluent could be collected after about 5 min. And about 2000 ml sample are collected, before the equipment get stopped. Finally nitrate acid solution at about 1 mol/L will be fed into the reactor to wash it after the reactor is cooled down to room temperature.

2.3 Reactor design

With the device design, the heating section and the reaction section will be described in more detail. First, the heating section will be described. In this study, the temperature of the reaction section was the temperature after the preheated water-ethanol mixed solvent and the sample solution were mixed, and the temperature of the water-ethanol mixed solvent immediately before the internal cooling water was set to 250 $^{\circ}\text{C}$. The enthalpy of water at 250 $^{\circ}\text{C}$ and 20 MPa is 2.16 MJ/kg, which is 215.67 kJ/min per hour when the flow rate is 100 g/min. On the other hand, the enthalpy of water at a temperature of 25 $^{\circ}\text{C}$ and 20 MPa is 0.13 MJ/kg, and when flowing at a flow rate of 20 g/min, it is 2.65 kJ/min per hour. Therefore, in order to mix the preheated water with the sample solution and rapidly mix them into a supercritical state at 250 $^{\circ}\text{C}$ and 20 MPa, it is necessary to provide a difference of 213.02 kJ/

min. Considering that the flow rate of the preheated water is 40 g/min, the preheated water needs to have an enthalpy of 2.66 MJ/kg. This corresponds to 280 °C under the condition of 20 MPa. Actually, it was experimentally confirmed that when the temperature of the preheated water reached 280 °C, the temperature of the reaction section reached 250 °C.

Next, the reaction section will be described. In this study, a swirl mixer made of SUS316 (inner diameter: 0.8 mm) was used to secure the Re number in the mixing section. Thereafter, the volume until the internal cooling water flows in was defined as the residence time, and the design was made so that the predetermined residence time was reached. As an example, Fig. 2-2 shows the reaction parts designed to have a residence time of 5 s, 10 s, and 20 s, respectively. And Table 2-2 shows the calculation results of the residence time of 5 s in each part. Table 2-3 shows the calculation results of the residence time of 10 s in each part. Table 2-4 shows the calculation results of the residence time of 20 s in each part. In order to prevent clogging of the particles, a 1/4 SUS316 T-shaped joint was used for the thermocouple connection portion and the cooling water introduction portion. The sum of these volumes gives a residence time of about 0.18 s. In addition, since the residence time in the mixing section and the reaction section 1 is about 0.018 s, the residence time in the reaction section 2 may be designed to be 4.8 s, 9.8s and 19.8s in total. The residence time was controlled by changing the volume of the reaction section 2 so as to achieve a predetermined residence time.

2.4 Analysis method

The collected particles were analyzed by XRD, TEM. The filtrate collected during the filtration was quantified for dissolved metal concentrations by UV-VIS. The following describes each analysis.

2.4.1 XRD

X-ray crystallography (XRC) is the experimental science determining the atomic and molecular structure of a crystal, in which the crystalline structure causes a beam of incident X-rays to diffract into many specific directions. By measuring the angles and intensities of these diffracted beams, a crystallographer can produce a three-dimensional picture of the density of electrons within the crystal. From this electron density, the mean positions of the atoms in the crystal can be determined, as well as their chemical bonds, their crystallographic disorder, and various other information. Since many

materials can form crystals—such as salts, metals, minerals, semiconductors, as well as various inorganic, organic, and biological molecules—X-ray crystallography has been fundamental in the development of many scientific fields. In its first decades of use, this method determined the size of atoms, the lengths and types of chemical bonds, and the atomic-scale differences among various materials, especially minerals and alloys.

The technique of single-crystal X-ray crystallography has three basic steps. The first—and often most difficult—step is to obtain an adequate crystal of the material under study. The crystal should be sufficiently large (typically larger than 0.1 mm in all dimensions), pure in composition and regular in structure, with no significant internal imperfections such as cracks or twinning. In the second step, the crystal is placed in an intense beam of X-rays, usually of a single wavelength (monochromatic X-rays), producing the regular pattern of reflections. The angles and intensities of diffracted X-rays are measured, with each compound having a unique diffraction pattern.[103] As the crystal is gradually rotated, previous reflections disappear and new ones appear; the intensity of every spot is recorded at every orientation of the crystal. Multiple data sets may have to be collected, with each set covering slightly more than half a full rotation of the crystal and typically containing tens of thousands of reflections. In the third step, these data are combined computationally with complementary chemical information to produce and refine a model of the arrangement of atoms within the crystal. The final, refined model of the atomic arrangement (crystal structure) is usually stored in a public database.

2.4.2 TEM

Transmission electron microscopy (TEM) is a microscopy technique in which a beam of electrons is transmitted through a specimen to form an image. The specimen is most often an ultrathin section less than 100 nm thick or a suspension on a grid. An image is formed from the interaction of the electrons with the sample as the beam is transmitted through the specimen. The image is then magnified and focused onto an imaging device, such as a fluorescent screen, a layer of photographic film, or a sensor such as a scintillator attached to a charge-coupled device.

And the size and morphology of the generated particles were observed with a transmission electron microscope (JEOL-2100, manufactured by JEOL Ltd.). For the preparation of the TEM sample, the collected particles were first ground in a mortar, then added to a very small amount of ethanol, and

dispersed by applying ultrasonic waves for about 5 minutes. About one drop of the dispersion was dropped on a copper microgrid and dried to prepare a TEM sample. The particle diameter counted 150 or more particles, performed image processing using ImageJ, and computed the average particle diameter.

2.4.3 UV-Vis

The concentration of Co ions in the filtered effluent are measured through the UV-vis method. Ultraviolet–visible spectroscopy (UV–Vis) refers to absorption spectroscopy or reflectance spectroscopy in part of the ultraviolet and the full, adjacent visible spectral regions. This means it uses light in the visible and adjacent ranges. The absorption or reflectance in the visible range directly affects the perceived color of the chemicals involved. In this region of the electromagnetic spectrum, atoms and molecules undergo electronic transitions. Absorption spectroscopy is complementary to fluorescence spectroscopy, in that fluorescence deals with transitions from the excited state to the ground state, while absorption measures transitions from the ground state to the excited state.

Then the value of concentration of Co ions in the filtered effluent are calculated following the Lambert–Beer law. The Lambert–Beer law relates the attenuation of light to the properties of the material through which the light is travelling. The law is commonly applied to chemical analysis measurements and used in understanding attenuation in physical optics, for photons, neutrons, or rarefied gases. In mathematical physics, this law arises as a solution of the BGK equation. A common and practical expression of the Beer-Lambert law relates the optical attenuation of a physical material containing a single attenuating species of uniform concentration to the optical path length through the sample and absorptivity of the species. This expression is:

$$A = \epsilon lc \quad (\text{Eq. 2-1})$$

ϵ : the molar attenuation coefficient or absorptivity of the attenuating species

l : the optical path length

c : the concentration of the attenuating species

2.5 Summary of this chapter

This chapter summarizes the reagents used, the experimental equipment, and the method of characterization of the prepared samples.

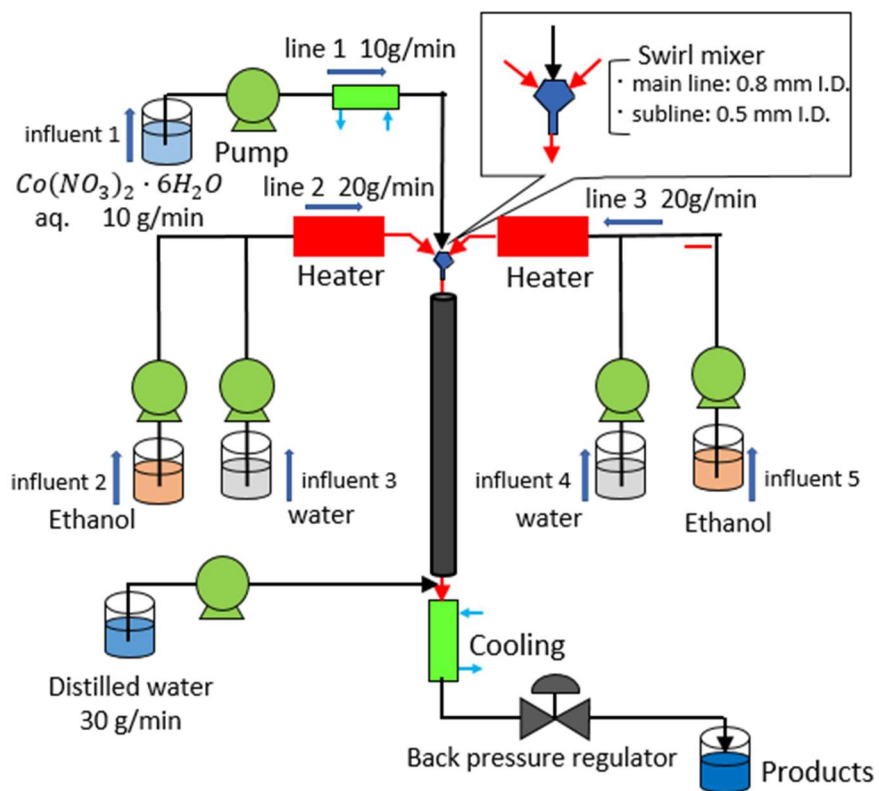


Fig. 2-1. Continuous flow reactor

Table. 2-1. Flow rate of each pump at different molar ratio of ethanol

ethanol ratio	effluent 1	effluent 2	effluent 3	effluent 4	efflurnt 5	(ml/min)
0	10	0	20	20	0	
0.1	10	7.09	14.4	14.4	7.09	
0.2	10	12.47	10.16	10.16	12.47	
0.3	10	16.68	6.84	6.84	16.68	
0.4	10	20.08	4.16	4.16	20.08	
0.5	10	22.87	2	2	22.87	
0.6	10	19.89	0.11	0.11	19.89	
0.8	5	28.9	0	0	28.9	

Table. 2-4. Continuous flow reactor design for reaction time at 20 s and calculation

	reactor1	union	reactor2	union	reactor3	union	reactor4												
mixer																			
inner diameter (r	0.8 inner diameter	1	1.3	3.87	4.8	9.4	4.8	3.87	4.8	3.05	4.8								
length (mm)	12 length	1/16	10.5 length	1/4	8.9 length	1/2	8.9 length	1/4	23.4	30	11.7								
volume (m ³)	6.03186E-09	7.854E-08	1.39E-08	5.88E-07	1.611E-07	2.08E-05	1.6E-07	5.88E-07	4.234E-07	2.2E-07	2.12E-07								
volume rate (m ³ /	1.2006E-06	1.2006E-06	1.2E-06	1.2E-06	1.201E-06	1.2E-06	1.2E-06	1.2E-06	1.201E-06	1.2E-06	1.2E-06								
resident time (s)	0.005024055	0.06541738	0.011608	0.489875	0.1394423	17.34084	0.13414	0.489875	0.3526887	0.18256	0.176344								
resident time																			
19.38252058																			

Chapter 3

3.1 Co ions conversion

In this section, conversions of cobalt ions at each water/ethanol molar ratio condition and different reaction time will be discussed.

3.1.1 Nanoparticle formation

Firstly, synthesis with only water at 250 °C, 20 MPa was conducted. When using only water as the solvent, no nanoparticle formation was observed at reaction time of 5 s. Based on this result, we have two hypothesis to explain it. The first one is that the reaction rate is too small at this temperature for to have any product. The other one is that this condition is not thermodynamic unstable enough to support any reaction of cobalt ions.

To check which of the hypothesis may explain this result better. The synthesis with only water at 250 °C, 20 MPa was then conducted at reaction time of 10 s and 20 s. Also no nanoparticle formation was observed at reaction time of 10 s and 20 s. Based on this result, the first hypothesis that the reaction rate is too small at this temperature for to have any product may be confirmed to be an inappropriate explanation, for the reason that even the reaction time was extended to 20 s, no reaction was observed and the conversion of cobalt ions still stayed at almost 0%.

As for the second hypothesis of this result, then the synthesis with 0.1 molar ratio of ethanol and 0.9 of water at 250 °C, 20 MPa was conducted at the reaction time of 20 s. At this condition, some white substance was observed in the effluent in reaction process, as shown in Fig. 3-1a, and part of them redissolved immediately after the reaction. After reaction stopped several hours, the collected effluent was put together with the effluent of reaction with only water, as shown in Fig. 3-1b, comparing with the effluent of reaction with only water, the effluent at this condition appears more turbid, which indicates that some substance was produced at this condition. And I tried to recover the substance from the solution by filtering it, but the amount of this substance was too small to collect.

Based on the result above, the hypothesis that this condition is not thermodynamic unstable enough to support any reaction of cobalt ions seems a reasonable explanation. To deeply explain about these results, a brief introduction about the classic nucleation theory is needed, as shown in (Eq. 3-1),

$$r_{crit} = \frac{2\gamma}{k_B T \ln(S)} \quad (\text{Eq. 3-1})$$

r_{crit} : Critical radius

γ : Surface energy

v : Molar volume

k_B : Boltzmann's constant

T : Temperature

S : Supersaturation

At the nanoparticle synthesis process, for the nucleus to participate, it has a smallest particle radius beyond which it will not dissolve again following the thermodynamic rules. This smallest radius is called critical radius. And the process for the nucleus to participate is called nucleation. In this equation, when reagent used is constant, the surface energy of nucleus also becomes constant, and also the molar ratio, so the critical radius only depends on the temperature and supersaturation of the solvent.

So in this experiment, when only water was used as solvent at temperature of 250 °C and pressure of 20 MPa condition, according to the property change of water along with the temperature increasing shown in Fig. 1-4, the dielectric constant of water is still much higher than that near the critical point, which lead to a relatively high solubility of cobalt ions even at this high temperature and high pressure condition. Thus the supersaturation and temperature are not large enough to produce a small critical radius for the cobalt nucleus to reach, and finally no nanoparticle formation was observed at this 250 °C and 20 MPa condition with only water. With the molar ratio of ethanol in the water-ethanol mixed solvent increased to 0.1, considering the relatively low permittivity of ethanol comparing with water at room temperature and lower critical temperature comparing with water, it is reasonable to infer that at 250 °C and 20 MPa condition (beyond the critical point of ethanol), ethanol has a much more lower permittivity than water at the same condition. By mixing 0.1 molar ratio of ethanol into water, permittivity of this mixed solvent will get lower comparing with pure water, causing a decreased solubility of cobalt ions, thus the supersaturation of cobalt ions got increased and produced a small critical radius enough for any cobalt substance to form, although the temperature stayed the same.

But the amount of substance formed is too small to be collect for any characterization and analysis,

experiments at ethanol molar ratio higher than 0.1 need to be conducted. This part will be discuss in next section.

3.1.2 Conversion

Synthesis with molar ratio of ethanol at 0.2 in the mixed solvent was conducted at 250 °C, 20 MPa and reaction time of 5 s. When the molar ratio of ethanol was increased to 0.2, color of the effluent become black and effluent appeared much more turbid compared with the effluent of reaction with 0.1 molar ratio of ethanol in the mixed solvent at reaction time of 20 s. After filtering the effluent, a big amount of black substance staying on the filter membrane was observed. Based on the phenomenon above, some nanoparticles formation was confirmed at this condition. And about the filtered effluent, a little bit pink color was still observed in this solution.

Then experiment at longer reaction time at 10 s was also conducted, and other conditions stayed the same. Similar phenomenon was observed at this reaction time. Color of the effluent become black and effluent appeared much more turbid compared with the effluent of reaction with 0.1 molar ratio of ethanol in the mixed solvent at reaction time of 20 s. After filtering the effluent, a big amount of black substance staying on the filter membrane was observed. Based on the phenomenon above, some nanoparticles formation was confirmed at this condition. And about the filtered effluent, also a little bit pink color was still observed in this solution.

Based on the results above, at 0.2 molar ratio of ethanol the cobalt substance was produced much more than the amount at 0.1 molar ratio of ethanol in the mixed solvent, at reaction time of 5 s, 10 s. Then considering the classical nucleation theory, for the temperature of this reaction always stayed the same, the drastic change in the amount of cobalt substance produced indicates that the supersaturation of cobalt ions in the mixed solvent with 0.2 molar ratio of ethanol increased drastically from that in the mixed solvent with 0.1 molar ratio of ethanol, which show the possibility that permittivity also decreased a lot from that in the mixed solvent with 0.1 molar ratio of ethanol. Then considering the situation of water that near the critical point of water, the physical property of water has a drastic change, water-ethanol mixed solvent as a similar polar fluid with hydrogen bond in it, it is reasonable to infer that the critical temperature of mixed solvent with 0.2 molar ratio of ethanol may be close to 250 °C at pressure of 20 MPa.

Then UV-Vis was used to measure the concentration of cobalt ions in the filtered effluent of reaction conducted at 0.2 molar ratio of ethanol and reaction time of 5 s, 10 s. And conversion was calculated based on the measured concentration and listed in table 3-1.

As shown in the table 3-1, the conversion of cobalt ions at 0.2 molar ratio of ethanol and reaction time of 5 s is 89.35%, this value increased a little bit to 91.14% at reaction time of 10 s. This means the cobalt ions did not get fully reacted at 0.2 molar ratio of ethanol and reaction time of 5 s and 10 s, some cobalt ions stayed unreacted.

About this result, also two hypothesis are supposed. The first one is that because of the conversion of cobalt ions increasing from reaction time of 5 s to 10 s, the reaction rate at this condition may not be so fast for the cobalt ions to get fully reacted. While the other hypothesis suggests that although the conversion increased from reaction time of 5 s to 10 s, the difference between these two conversion values is not so large, which indicates that this conversion around 90% may be the equilibrium conversion for cobalt ions at this 0.2 molar ratio of ethanol condition.

To check this point, experiment at reaction time of 20 s was also conducted, and other conditions still stayed the same. Similar phenomenon with another two reaction time of 5 s and 10 s was also observed at this reaction time. And the conversion of cobalt ions stayed at 91.38%, almost the same with that at reaction time of 10 s. This result rejected the first hypothesis and confirmed the hypothesis that equilibrium conversion for cobalt ions at this 0.2 molar ratio of ethanol condition stays around 90%.

Then to increase the conversion further and study how the equilibrium conversion are determined, experiments at 0.3 molar ratio of ethanol in the mixed solvent and reaction time at 5 s, 10 s, and 20 s are conducted. Experiment at 0.4 molar ratio of ethanol in the mixed solvent and reaction time at 10 s is also conducted. Similar phenomenon with another reactions at 0.2 molar ratio of ethanol was observed at each reaction time. While cobalt ions conversions of these experiments changed. The conversions of experiments at 0.3 molar ratio of ethanol and reaction time at 5 s, 10 s has almost the same values at 97.9%, the conversion of experiment at 0.3 molar ratio of ethanol and reaction time at 20 s is a little bit higher and reached 98.55%. And the conversion of experiment at 0.4 molar ratio of ethanol and reaction time at 20 s got lower again at 92.28%.

Based on the conversion results in last paragraph, two things are noticed. Firstly, 0.3 molar ratio of

ethanol in the mixed solvent may supply the highest cobalt ions conversion for this nanoparticle reaction. And another point is that there are at least two factors which affect the particle synthesis process with the ratio of ethanol changing in the mixed solvent because of the tendency that the conversion of cobalt ions went higher from 0.2 molar ratio of ethanol to 0.3 and decreased from 0.3 molar ratio of ethanol to 0.4.

In this section, we talked about the conversions of cobalt ions at a relatively low molar ratio of ethanol and the reason why the experiment result changes from no nanoparticles formation with only water to a big amount of cobalt formation when the ratio is upper than 0.2. To further study about the factors that affect the particle synthesis process with the ratio of ethanol changing in the mixed solvent, experiment need to be conducted at higher molar ratio of ethanol up to 0.5. And results will be discussed together with the characterization of nanoparticles synthesized at each condition in next section.

3.2 Lower ethanol ratio range

In this section, characterization of nanoparticles synthesized at molar ratios of ethanol ranges from 0.2 to 0.5 will be discussed, and the size and shape of the nanoparticles will also be covered, not only nucleation process, but also crystal growth process will be included into the discussion. So a brief introduction of the classical crystal growth theory is needed.

3.2.1 Classical crystal growth theory

The growth of nanoparticles is dependent on two mechanisms: the surface reaction and the monomer's diffusion to the surface [52]. To model growth by diffusion Fick's first law, (Eq. 3-2) can be applied, Figure 3-2.

$$J = 4\pi x^2 D \frac{dC}{dx} \quad (\text{Eq. 3-2})$$

r: Particle radius.

J: The total flux of monomers passing through a spherical plane with radius *x*.

D: Diffusion coefficient.

C: Concentration at a distance *x*.

Fick's first law can be rewritten, (Eq. 3-3), for the case of a nanoparticle within solution, Figure 3-2.

$$J = \frac{4\pi Dr(r+\delta)}{\delta} (C_b - C_i) \quad (\text{Eq. 3-3})$$

δ : Distance from the particle surface to the bulk concentration of monomers within solution,

C_b : the bulk concentration of monomers within the solution.

C_i : The concentration of monomers at the solid/ liquid interface.

C_r : The solubility of the particle.

As J is constant irrespective of x due to the steady state of the solute diffusion, integration of $C(x)$ from $(r + \delta)$ to r gives (Eq. 3-4).

$$J = 4\pi Dr(C_b - C_i) \quad (\text{Eq. 3-4})$$

A similar equation can be written for the rate of surface reaction "k", (Eq. 3-5). The rate of the surface reaction is assumed to be independent of particle's size.

$$J = 4\pi r^2 k(C_i - C_r) \quad (\text{Eq. 3-5})$$

From (Eq. 3-4) and (Eq. 3-5) there are two limiting factors: either the diffusion of monomers to the surface or the rate of reaction of these monomers on the surface. If diffusion is the limiting factor then the change in particle size with time is given by (Eq. 3-6).

$$\frac{dr}{dt} = \frac{Dv}{r} (C_b - C_r) \quad (\text{Eq. 3-6})$$

Similarly if the surface reaction is the limiting factor then (Eq. 3-4) and (Eq. 3-5) can be approximated to (Eq. 3-7).

$$\frac{dr}{dt} = kv(C_b - C_r) \quad (\text{Eq. 3-7})$$

When the growth of nanoparticles is neither diffusion nor surface reaction controlled, the increase in particle's radius with time is written as (Eq. 3-8).

$$\frac{dr}{dt} = \frac{Dv(C_b - C_r)}{r + D/k} \quad (\text{Eq. 3-8})$$

Strictly speaking, the solubility of nanoparticles is not independent of particle's size and according to Gibbs–Thomson relation, (Eq. 3-9). A spherical particle has an extra chemical potential $\Delta\mu = 2\gamma v/r$. Then C_r is expressed as a function of r .

$$C_r = C_b \exp\left(\frac{2\gamma v}{rk_B T}\right) \quad (\text{Eq. 3-9})$$

v : The molar volume of the bulk crystal.

C_b : Concentration of the bulk solution.

For the growth of NPs, a general expression (Eq. 3-6) can be produced through combining (Eq. 3-10) and (Eq. 3-8). [53]

$$\frac{dr^*}{d\tau} = \frac{s - \exp\left(\frac{1}{r_{cap}}\right)}{r_{cap} + K} \quad (\text{Eq. 3-10})$$

Where the three dimensionless constants are defined as follows:

$$r_{cap} = \frac{RT}{2\gamma v} r \quad (\text{Eq. 3-11})$$

$$\tau = \frac{k_B^2 T^2 D C_b}{4\gamma^2 v} \quad (\text{Eq. 3-12})$$

$$K = \frac{k_B T D}{2\gamma k} \quad (\text{Eq. 3-13})$$

$2\gamma v/k_B T$: The capillary length

K: the Damköhler number.

The Damköhler number indicates whether the reaction is diffusion or reaction rate dependent. If $D \ll 1$ then the diffusion rate dominates over the surface reaction.

3.2.2 Nanoparticle size

The TEM images of samples synthesized at 0.2 molar ratio of ethanol at reaction time of 5 s are shown in Fig.3-3. From the images, it is shown that almost all of the nanoparticles observed have cubic shape, and the size distribution of these nanoparticles statistic by ImageJ have an average size at 120.8 nm, with a standard deviation at 27.8 nm. And according to the XRD results in Fig. 3-10a, the XRD patterns show all the peaks of Co_3O_4 nanoparticles. These results indicated that the nanoparticle synthesized at this condition are almost all cubic Co_3O_4 nanoparticles, and have the lattice constants shown in the Fig. 3-13a.

And the TEM images of samples synthesized at 0.2 molar ratio of ethanol at reaction time of 10 s are shown in Fig.3-4. Almost the same with that at reaction time of 5 s, almost all of the nanoparticles observed have cubic shape, and the size distribution of these nanoparticles statistic by ImageJ have an average size at 99.3 nm, with a standard deviation at 28.0 nm. And according to the XRD results in Fig. 3-11a, the XRD patterns show all the peaks of Co_3O_4 nanoparticles. These results indicated that the nanoparticle synthesized at this condition are also almost all cubic Co_3O_4 nanoparticles, and the same with particles in reaction time of 5 s, have the lattice constants shown in the Fig. 3-13a

Almost the same results are also observed in the nanoparticles synthesized at reaction time of 5 s (Fig. 3-5), except that the size distribution of the nanoparticles at this condition changed to average size at 104.9 nm, with a standard deviation at 36.2 nm.

Now let's have a look at the cobalt nanoparticles synthesized at these three conditions. Firstly the average size of nanoparticles decreased from 120 nm to 99.3 nm, from reaction time of 5 s to 10 s, then increased to 104.9 nm from reaction time of 10 s to 20 s. About this point, considering the almost stable conversion values around 90% at these conditions, it is indicated that at 0.2 molar ratio of ethanol in the mixed solvent, the cobalt nanoparticle synthesis reaction has reached its equilibrium

state before reaction time of 5 s at 250 °C 20 MPa condition.

Then when the molar ratio of ethanol in the mixed solvent was increased to 0.3, the TEM images of samples synthesized at reaction time of 5 s, 10 s, and 20 s, are shown in Fig. 3-6, Fig. 3-7, and Fig. 3-8, respectively. Also, all of these samples are observed to have the same cubic shape. And according to the XRD results in Fig. 3-10b, Fig. 3-11b, and Fig. 3-12b, it is confirmed that at all of these reaction times, Co_3O_4 nanoparticles are synthesized. As for the particle size of these three samples, statistic by ImageJ, at reaction time of 5 s, the average particle size reached 82.6 nm, with a standard deviation at 38.3 nm. At reaction time of 10 s, the average particle size reached 90.1 nm, with a standard deviation at 39.9 nm, and at reaction time of 20 s, the average particle size reached 90.3 nm, with a standard deviation at 33.9 nm.

Based on the results in last paragraph, considering the almost stable conversion values around 98% at these conditions, it is also indicated that at 0.3 molar ratio of ethanol in the mixed solvent, the cobalt nanoparticle synthesis reaction has reached its equilibrium state before reaction time of 5 s at 250 °C 20 MPa condition.

Then let's consider the two equilibrium state at 0.2 molar ratio of ethanol and 0.3 molar ratio of ethanol in the mixed solvent. Comparing with the cobalt nanoparticles synthesized at 0.2 molar ratio of ethanol, the cobalt nanoparticles synthesized at 0.3 molar ratio of ethanol has a smaller average particle size and the synthesis reaction has a higher cobalt ions conversion. And from the TEM images of samples synthesized at 0.3 molar ratio of ethanol, more particles with a particles size as small as 50 nm can be observed than that of samples synthesized at 0.2 molar ratio of ethanol.

Based on the classic nucleation theory, the higher molar ratio of ethanol of 0.3 comparing with 0.2 brings a lower permittivity of the mixed solvent, which caused a lower solubility of cobalt ions and a higher supersaturation, thus a smaller critical radius. And at this smaller critical radius, nucleation process occurred more than that of 0.2 molar ratio of ethanol, finally caused a higher conversion of cobalt ions at the equilibrium state of synthesis reaction at 0.3 molar ratio of ethanol. About the larger average particle size of samples synthesized at 0.2 molar ratio of ethanol, it is explained by the Fig.1-2 that at a lower supersaturation degree, the particles always tend to crystal growth instead of nucleation.

3.2.2 Nanoparticle shape

In last section, we mentioned that there are at least two factors which affect the particle synthesis process with the ratio of ethanol changing in the mixed solvent because of the tendency that the conversion of cobalt ions went higher from 0.2 molar ratio of ethanol to 0.3 and decreased from 0.3 molar ratio of ethanol to 0.4. And we have talked about the reason that how the conversion is increased and the relation between the increase of cobalt ions conversion with the cobalt nanoparticle size variation in last part of this section. In this part, we will focus on the other factor that may bring effects to the conversion of nanoparticle synthesis and the relation with the shape of the nanoparticles.

The TEM images of samples synthesized at 0.4 molar ratio of ethanol at reaction time of 10 s are shown in Fig.3-9. From the images, it is shown that almost all of the nanoparticles observed have cubic shape, but different with the nanoparticles synthesized at ethanol molar ratio of 0.2, 0.3, several particles with a broken structure could also be observed. And the size distribution of these nanoparticles statistic by ImageJ have an average size at 101.9 nm, with a standard deviation at 44.4 nm. And according to the XRD results in Fig. 3-11c, the XRD patterns show all the peaks of Co_3O_4 nanoparticles. These results indicated that the nanoparticle synthesized at this condition are almost all cubic Co_3O_4 nanoparticles, and have the lattice constants shown in the Fig. 3-13a.

Then when the molar ratio of ethanol in the mixed solvent was increased to 0.5, the TEM images of samples synthesized at reaction time of 5 s and 10 s, are shown in Fig. 3-15, and Fig. 3-16, respectively. Different from all of these samples synthesized at lower molar ratio of ethanol the shape of which are almost cubic, most of the cobalt nanoparticles synthesized at 0.5 molar ratio of ethanol are observed to have octagonal or round shape. And according to the XRD results in Fig. 3-10c and Fig. 3-11d, it is confirmed that at all of these reaction times, Co_3O_4 nanoparticles are synthesized. And the two samples have the same lattice constant as shown in Fig. 3-13b, which is a little bit larger than that of the cubic particles synthesized at lower molar ratio of ethanol. About the particle size of these two samples, statistic by ImageJ, at reaction time of 5 s, the average particle size reached 101.0 nm, with a standard deviation at 26.7 nm. At reaction time of 10 s, the average particle size reached 95.2 nm, with a standard deviation at 31.5 nm.

At the same molar ratio of ethanol, and reaction time was increased to 20 s, as shown in Fig. 3-17, unlike the octagonal or round shape nanoparticle are both observed at reaction time of 5 s and 10 s,

only octagonal particle could be observed. The same with the two samples synthesized at reaction time of 5 s and 10 s, this sample also have the lattice constant as shown in Fig. 3-13b. According to the XRD results in Fig. 3-12c, it is also confirmed that at reaction times of 20 s, Co_3O_4 nanoparticles are synthesized. And the average particle size reached 105.9 nm, with a standard deviation at 28.2 nm.

Firstly, let's focus on the characterization results of nanoparticles synthesized at reaction time of 5 s, 10 s, and 20 s, at 0.5 molar ratio of ethanol. Although the three samples have a similar average particle size, unlike the sample of each reaction time at lower molar ratio of ethanol that they have a stable cobalt ions conversion and almost the same cubic shape, on the one hand, the conversion of cobalt ions at 0.5 molar ratio of ethanol condition increased from a relatively low value at 58.08% to 64.57% from reaction time of 5 s to 10 s, then increased drastically to 95.06% from reaction time of 10 s to 20 s, which means at reaction time of 5 s and 10 s, the reaction is still far away to reach the equilibrium state of 0.5 molar ratio of ethanol condition. On the other hand, the shape of nanoparticles synthesized at this condition also changed from both of octagonal or round shape to only octagonal, and the edge of the particles also got sharper, it can be inferred that the round nanoparticles may play the role of an intermediate state of the octagonal shape nanoparticles. These two facts indicated that the cobalt nanoparticle synthesis has much more lower reaction rate and reach the equilibrium state of 0.5 molar ratio of ethanol condition at almost reaction time of 20 s.

Based on the results and discussion above, the two factor that may bring effect to the conversion of cobalt ions at the molar ratio of ethanol in the mixed solvent range from 0.2 to 0.5 become clear. The first factor are located in the permittivity of the high temperature and high pressure mixed solvent, which is directly connected to the supersaturation degree of cobalt ions in the solvent, and finally affect the conversion of cobalt ions at the equilibrium state, just as discussed in last section. And the second factor point to the reaction rate of the nanoparticle synthesis, when the molar ratio of ethanol is increased from 0.4 to 0.5, the reaction rate got much slower to reach the equilibrium state, thus the conversion got decreased.

As for the deep reason of the reaction rate change, we need to go back to the classical crystal growth theory. In this theory, the crystal growth process is divided to two types, diffusion controlled and surface reaction controlled. In the reaction of cobalt nanoparticles synthesis, water works not only as a part of the solvent, but also acts as one of the reagents in the hydrogenation reaction of cobalt ions,

as the molar ratio of ethanol goes as high as 0.5, crystal growth switches to a diffusion controlled process, the access to the reagent of water dominate the reaction rate.

Of course the shape change from the cubic particles to octagonal particles in the equilibrium state along with the molar ratio of ethanol increased from 0.4 to 0.5 can't be overlooked. It is directly caused by the slower growth rate of (1 1 1) face of the cubic particles. But about the explanation about how the ethanol slow down the growth of (1 1 1) face still need to be studied.

In last two sections, it is observed that at 0.7/0.3 w/e ratio, Co has a higher conversion than that of 0.8/0.2 w/e ratio, and particle size of NPs synthesized at 0.7/0.3 w/e ratio is also smaller than that at 0.8/0.2 w/e ratio condition. According to the classical nucleation theory, higher supersaturation degree of metal ions tends to promote the nucleation process and at lower supersaturation degree condition, the crystal growth process dominates the NPs synthesis. Comparing with water, ethanol has lower permittivity, which may cause lower solubility of Cobalt ions in the solvent. At the high temperature and high pressure condition (250°C, 20MPa), the solubility of Cobalt ions decreases with the ratio of ethanol in the mixed solvent increasing, which may cause a higher supersaturation degree of cobalt ions, resulted in the higher conversion of cobalt precursor and smaller particle of Co₃O₄ nanoparticles.

As for the octagonal and round particles synthesized at 0.5/0.5 w/e ratio condition, they have larger lattice constant than the cubic particles but the same XRD patterns, which means the crystal structure of octagonal and round particles differ from the cubic particles. Then considering the conversion result in Table 1 that unlike almost the same conversions at all of the reaction time (5, 10 20 s) for 0.8/0.2 and 0.7/0.3 w/e ratio, the conversion at 0.5/0.5 w/e ratio rises drastically from 10 to 20 seconds, this indicates that reaction rate of NPs synthesis at 0.5/0.5 w/e ratio is slower than lower ethanol condition. But the slower growth of (1 1 1) face of NPs at 0.5/0.5 w/e ratio needs further research.

Till now, the effect of mixing ethanol into water as solvent to the cobalt nanoparticle synthesis at a relatively low molar ratio has been discussed. About what changes in the process of cobalt nanoparticle synthesis will happen at a molar ratio of ethanol higher than 0.5, the experiments result will be described and discussed in next section.

3.3 Higher ethanol ratio range

In this section, the experiments results at a molar ratio of ethanol higher than 0.5 will be described and discussed.

3.3.1 Valance number change of cobalt oxide nanoparticles

As the molar ratio of ethanol in the mixed solvent was increased to 0.6, the TEM images of samples synthesized at reaction time of 5 s, 10 s, and 20 s, are shown in Fig. 3-18, Fig. 3-19, and Fig. 3-20, respectively. At reaction time of 5 s, only few particles are observed and most substance seems amorphous materials. And according to the XRD results in Fig. 3-25a, no clear peaks could be observed, this is consistent with the amorphous materials observed at TEM. At reaction time of 10 s, two types of particles are seen in the image. Then according to the XRD results in Fig. 3-25b, both peaks of Co_3O_4 and CoO are observed, which means at reaction time of 10 s, Co_3O_4 nanoparticles and Co are both synthesized. The lattice constant of the Co_3O_4 nanoparticle is the same as the octagonal particles synthesized at 0.5 molar ratio of ethanol, as shown in Fig. 3-13b. The lattice constant of the CoO nanoparticle is shown in Fig. 3-13c. As the reaction time increased to 20 s, octagonal particles appeared in the image. Then according to the XRD results in Fig. 3-25b, most of the peaks in the XRD pattern belong to Co_3O_4 and only a broad peak points to CoO . Which means Co_3O_4 is the dominate composition of the product. And the lattice constant of this Co_3O_4 nanoparticle is the same as the octagonal particles synthesized at 0.5 molar ratio of ethanol, as shown in Fig. 3-13b.

Then when the molar ratio of ethanol in the mixed solvent was increased to 0.5, the TEM images of samples synthesized at reaction time of 10 s and 20 s, are shown in Fig. 3-21, and Fig. 3-22, respectively. Different from all of these samples synthesized at lower molar ratio of ethanol the shape of which are almost cubic, octagonal or round shape. Most of the cobalt nanoparticles synthesized at 0.8 molar ratio of ethanol are observed to be rectangle or ladder-shape. And according to the XRD results in Fig. 3-23c and Fig. 3-24c, it is confirmed that at all of these reaction times, CoO nanoparticles are synthesized. And the two samples have the same lattice constant as shown in Fig. 3-13c, which is also the same as the CoO synthesized at 0.6 molar ratio and reaction time of 10 s.

Focusing on the XRD results shown in Fig. 3-23, and Fig. 3-24, it is known that at reaction time of 10 s and 20 s, the composition of synthesized nanoparticles always changes from Co_3O_4 to CoO with

the molar ratio of ethanol in the mixed solvent increased from 0.5 to 0.8. And comparing with Co_3O_4 , the valence number of cobalt in CoO is lower, which means a relatively reduced substances are produced along with the molar ratio of ethanol in the mixed solvent increased from 0.5 to 0.8.

Based on the results in this section, it is inferred that at 250°C 20MPa, higher ethanol ratio (over 0.5 molar ratio) of water-ethanol mixed solvent could provide a more reductive environment for Cobalt oxidant NPs synthesis.

3.3.2 Reaction time change at 0.6 molar ratio of ethanol condition.

And some special experiments results need to be noticed along with the Reaction time change at 0.6 molar ratio of ethanol condition.

Fig. 3-25 shows the XRD results of samples synthesized at 0.6 molar ratio of ethanol, 5 s, 10 s, 20 s reaction time respectively. At 5 s, both the peaks of Co_3O_4 and CoO are not clear, which indicates that amorphous materials may be produced at this condition, this is consistent with the results shown in Fig 6a. And when the reaction time is extended to 10s, clear peaks of Co_3O_4 and CoO appeared in the XRD pattern of this sample. As shown in the TEM image Fig 6b, both Co_3O_4 and CoO NPs could be observed. While when reaction time was set to 20 s, peaks of Co_3O_4 became sharper than shorter reaction time, peaks of CoO got broader. This means at 0.4/0.6 w/e ratio, CoO NPs appeared at 10s reaction time and almost disappeared at 20 s.

Based on the results in last part of this section, higher ethanol ratio (over 0.5 molar ratio) of water-ethanol mixed solvent could provide a more reductive environment for Cobalt oxidant NPs synthesis. The results at reaction time of 5 s and 10 s are consistent with this inference above, while the result that peaks of CoO got broader also shows another possibility that CoO may play the role as intermediate material at the process of Co_3O_4 NPs synthesis in this condition.

In this section, firstly it is indicated that at 250°C 20MPa, higher ethanol ratio (over 0.5 molar ratio) of water-ethanol mixed solvent could provide a more reductive environment for Cobalt oxidant NPs synthesis. About the disappearance of CoO at condition 0.4/0.6 w/e ratio 20 s, it shows the possibility that CoO may play the role as intermediate material at the process of Co_3O_4 NPs synthesis in this condition, although this point still need further study.

3.4 Summary of this chapter

In this chapter, the results of experiments conducted at different molar ratio of ethanol in the water-ethanol mixed solvent and different reaction time have been discussed, and some inferences have been made, although part of them still need further study.

Table. 3-1. Conversion of Co ions in Cobalt oxide NPs synthesis at different w/e ratio, 250°C, 20 MPa.

conversion	5 s	10 s	20 s
0.8/0.2 w/e	89.35%	91.14%	91.38%
0.7/0.3 w/e	97.90%	97.97%	98.55%
0.6/0.4 w/e		92.28%	
0.5/0.5 w/e	58.08%	64.57%	95.06%
0.4/0.6 w/e	32.24%	37.45%	41.51%
0.2/0.8 w/e		31.62%	59.26%



Fig. 3-1. The phenomenon happened in the process of reaction at ethanol ratio 0.1, a) effluent of this reaction, b) comparing between effluent of ethanol ratio at 0 and 0.1.

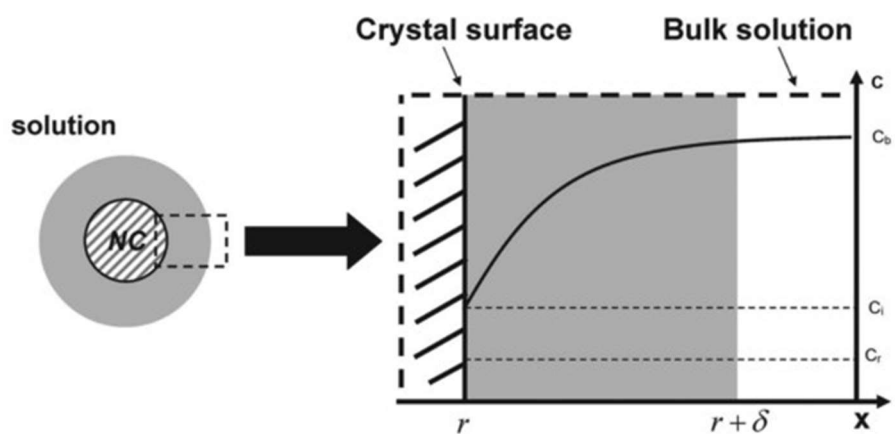


Fig. 3-2. Schematic illustration of diffusion layer structure near the surface of a nanocrystal (left) and plot for the monomer concentration as a function of distance x (right). The shaded area indicates the diffusion layer. [55]

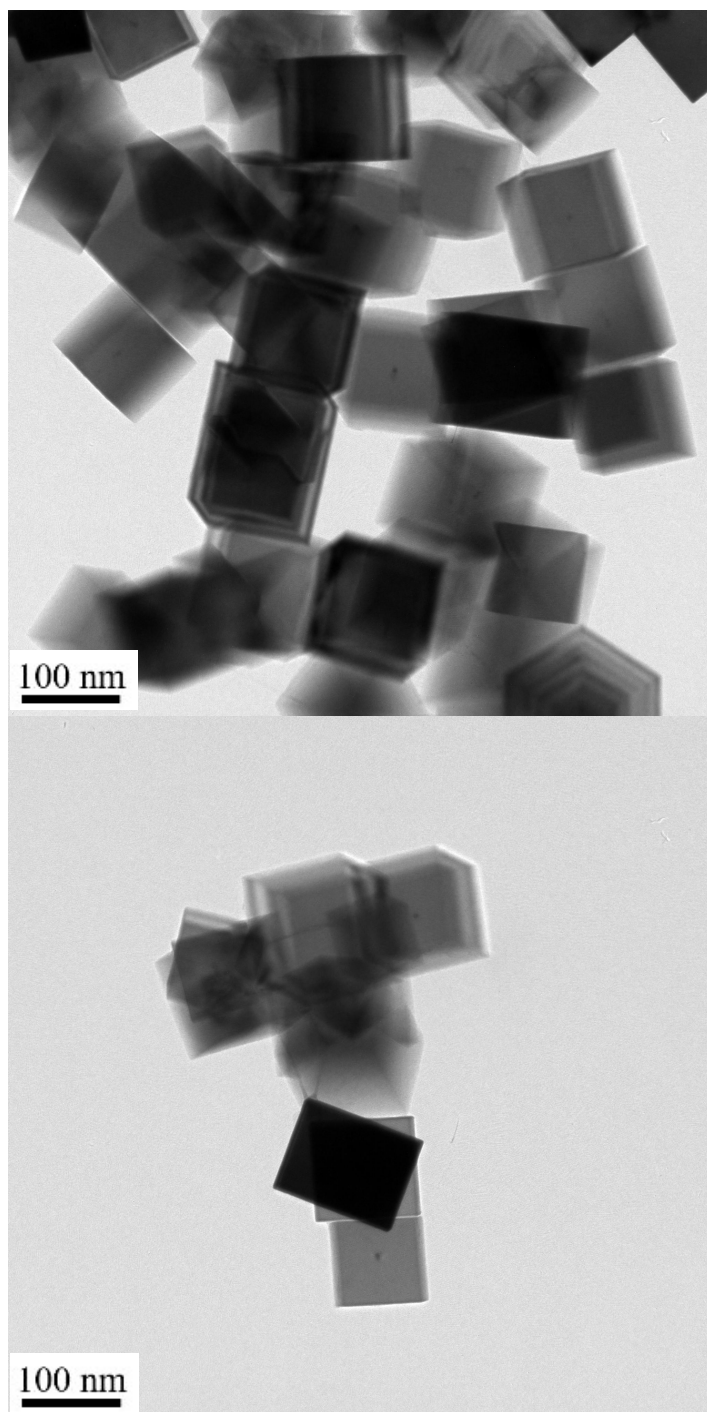


Fig. 3-3. Cobalt oxide nanoparticles synthesized at reaction time of 5 s, 0.2 molar ratio of ethanol.

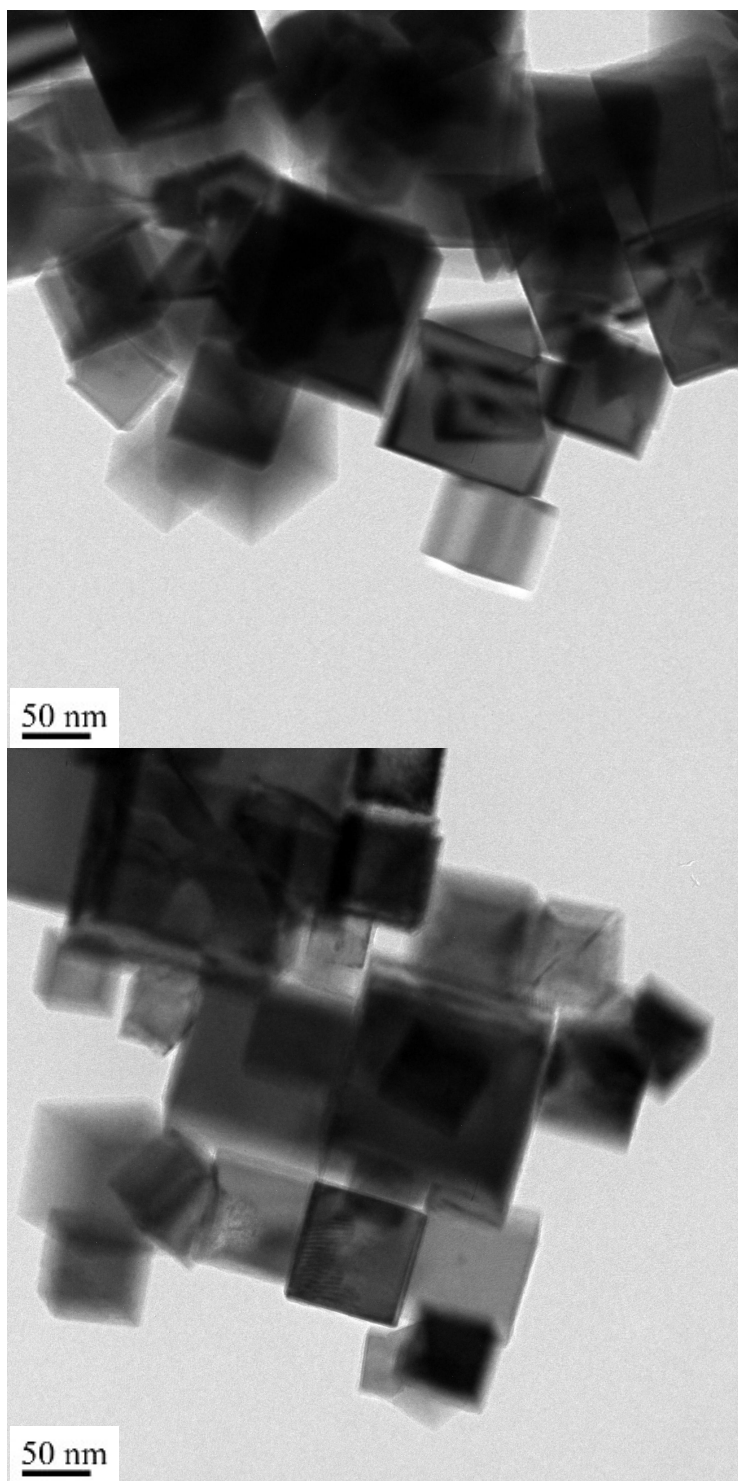


Fig. 3-4. Cobalt oxide nanoparticles synthesized at reaction time of 10 s, 0.2 molar ratio of ethanol.

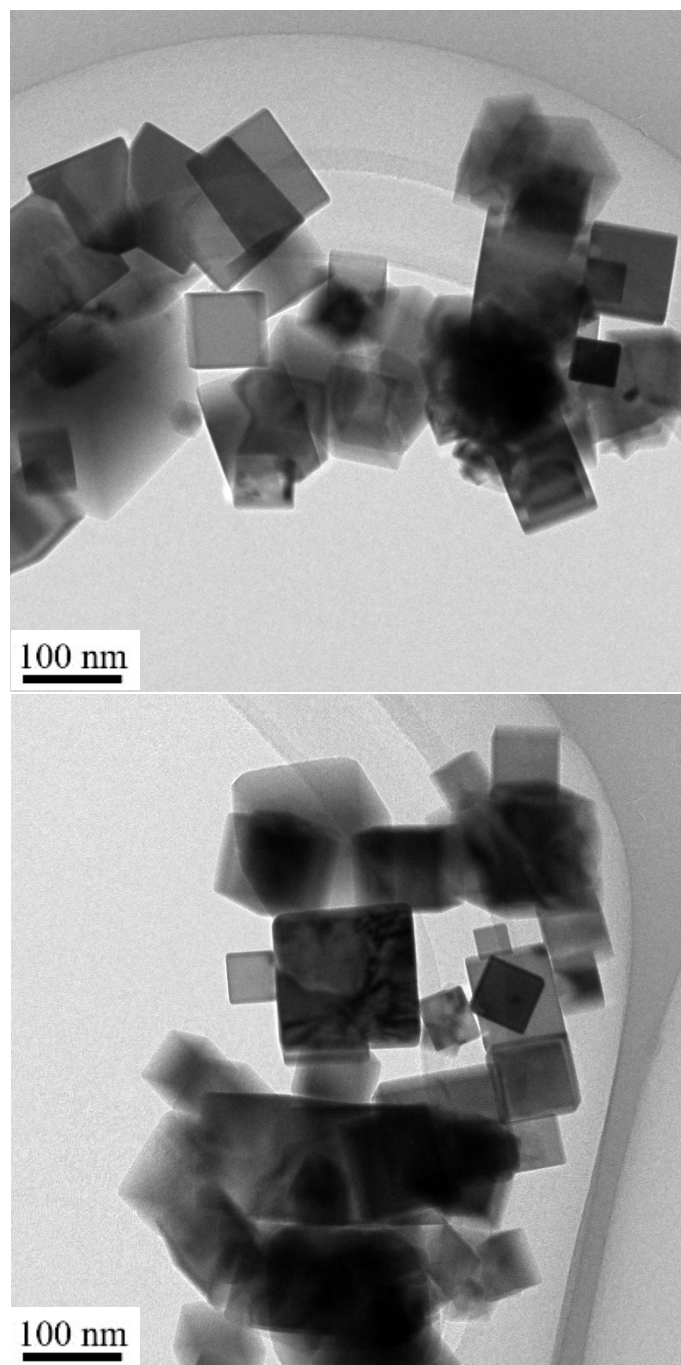


Fig. 3-5. Cobalt oxide nanoparticles synthesized at reaction time of 20 s, 0.2 molar ratio of ethanol.

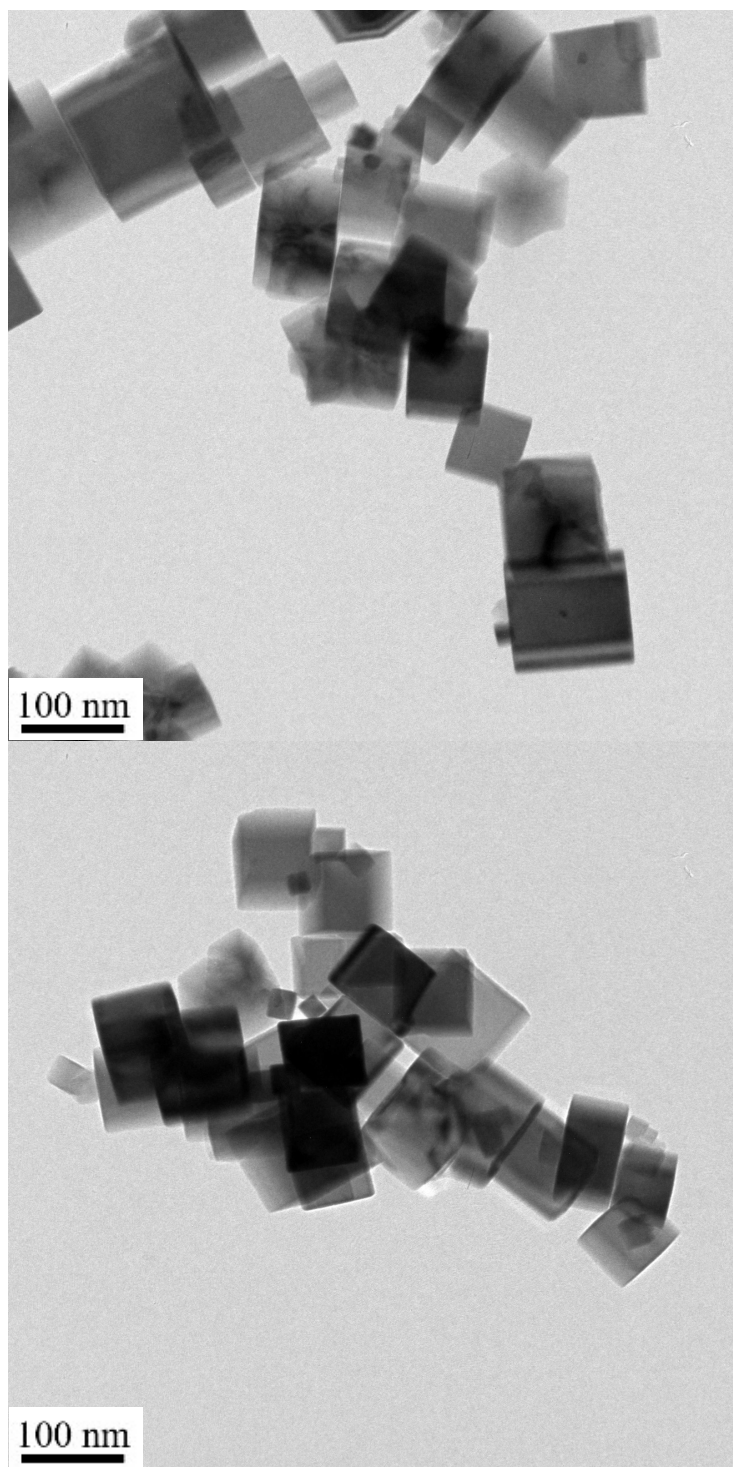


Fig. 3-6. Cobalt oxide nanoparticles synthesized at reaction time of 5 s, 0.3 molar ratio of ethanol.

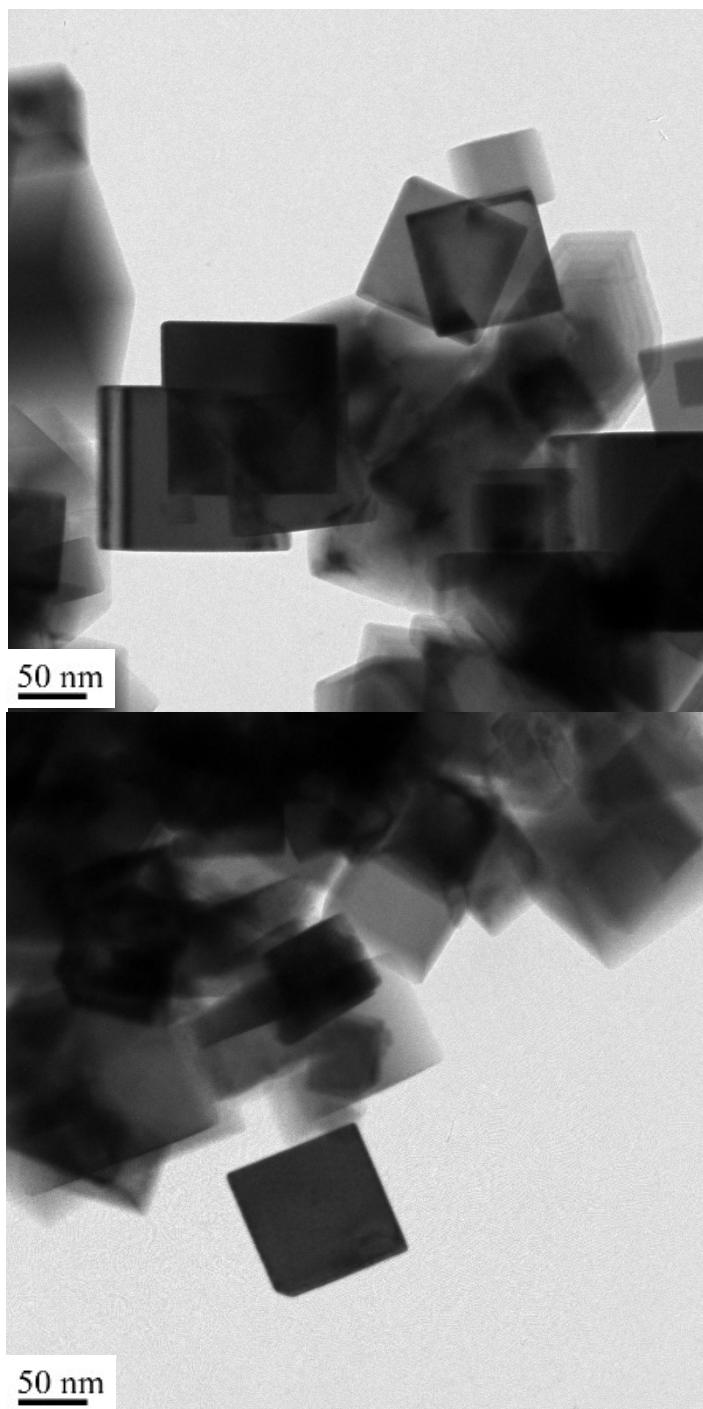


Fig. 3-7. Cobalt oxide nanoparticles synthesized at reaction time of 10 s, 0.3 molar ratio of ethanol.

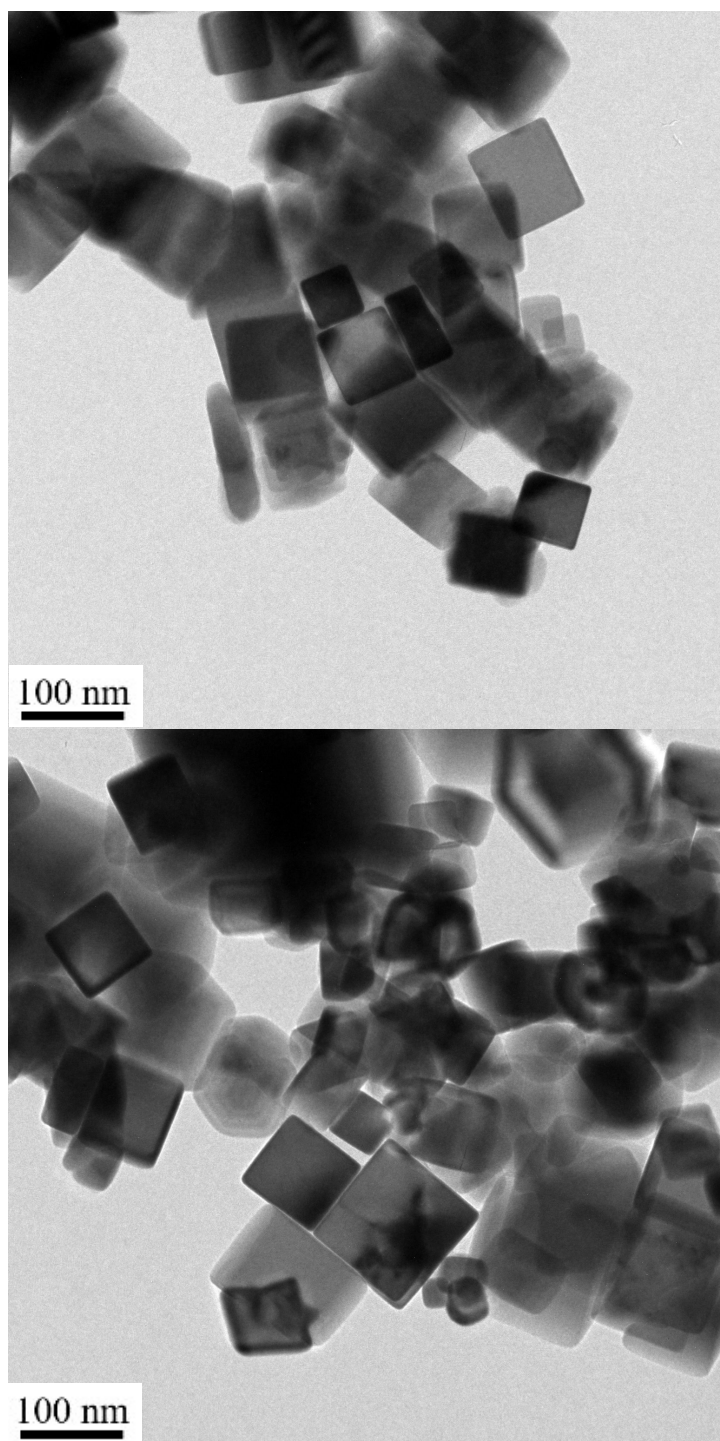


Fig. 3-8. Cobalt oxide nanoparticles synthesized at reaction time of 20 s, 0.3 molar ratio of ethanol.

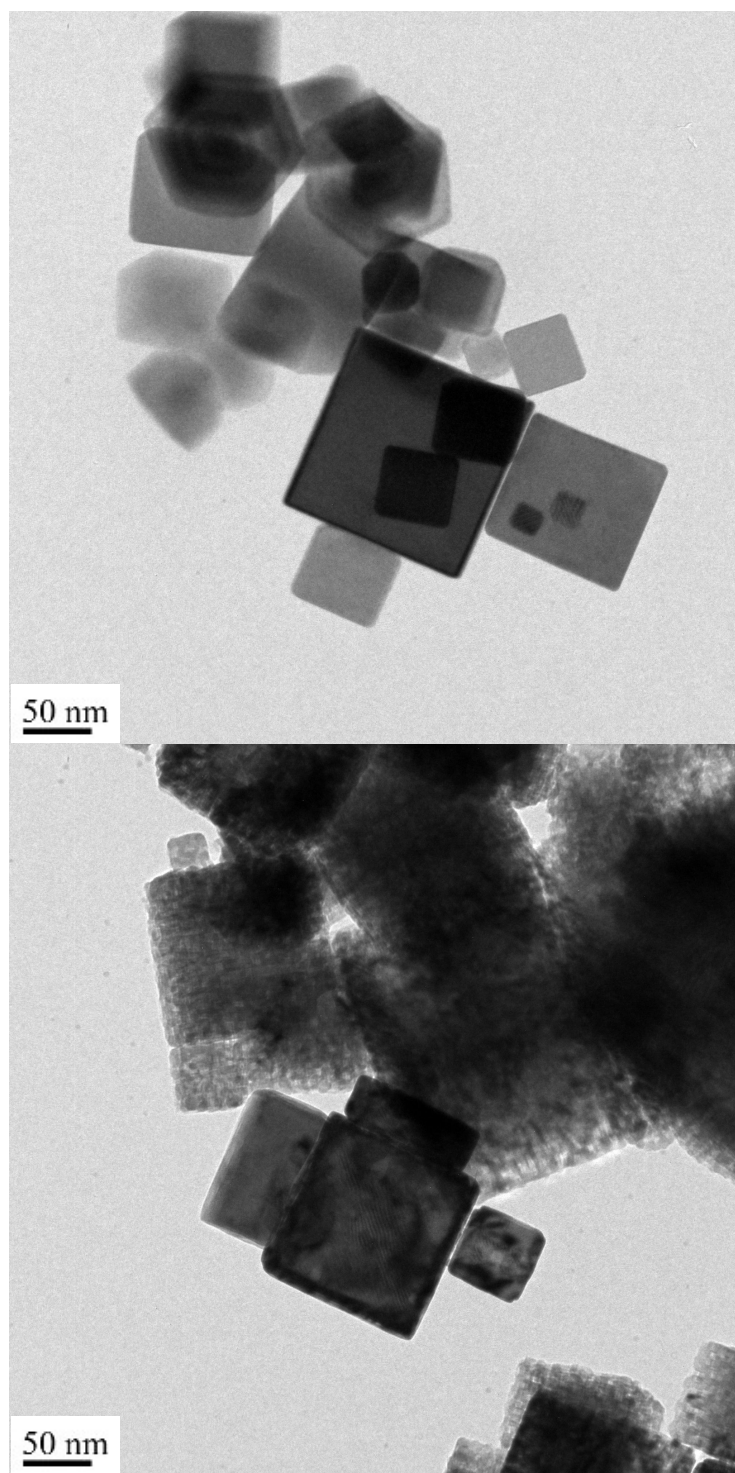


Fig. 3-9. Cobalt oxide nanoparticles synthesized at reaction time of 10 s, 0.4 molar ratio of ethanol.

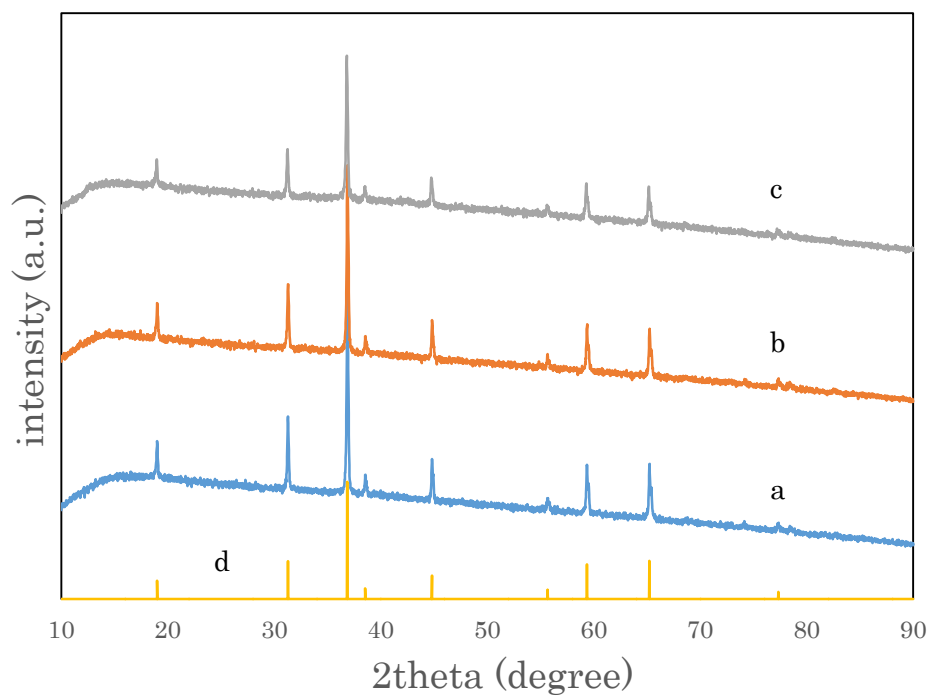


Fig. 3-10. XRD results for Cobalt oxide NPs synthesized at lower w/e ratio, 250°C, 20 MPa, 5s. a. 0.8/0.2, b. 0.7/0.3, c. 0.5/0.5, d, peaklist of Co₃O₄.

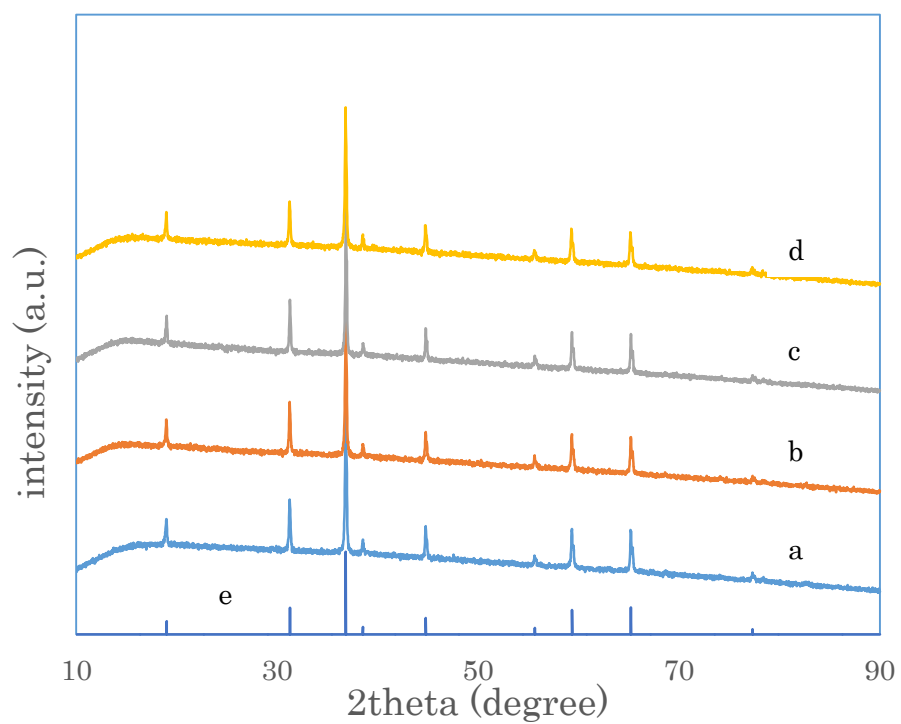


Fig. 3-11. XRD results for Cobalt oxide NPs synthesized at lower w/e ratio, 250°C, 20 MPa, 10s. a. 0.8/0.2, b. 0.7/0.3, c. 0.6/0.4, d. 0.5/0.5, e, peaklist of Co_3O_4 .

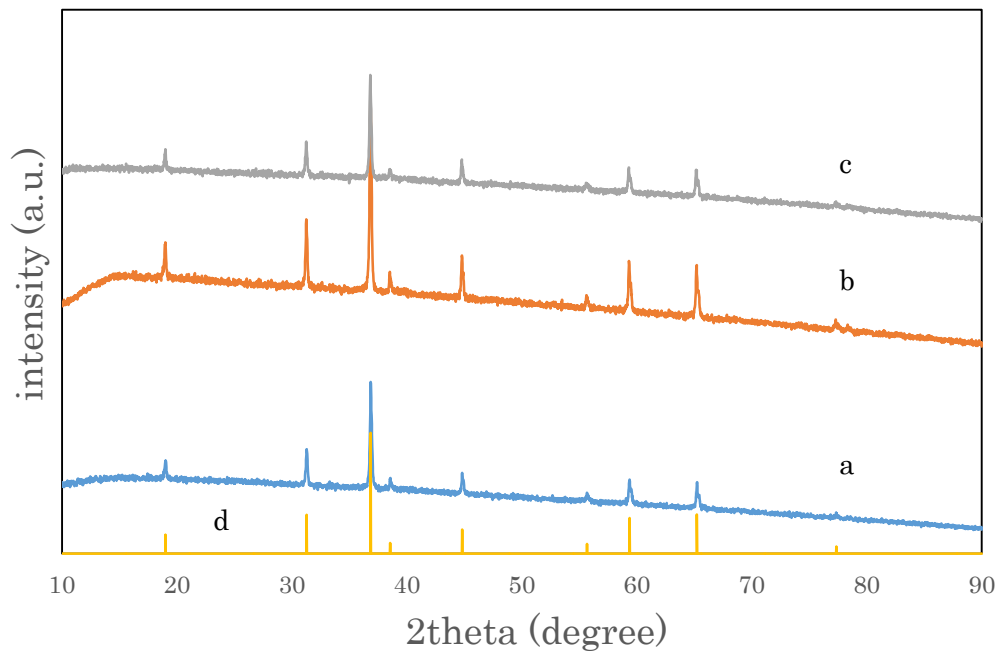


Fig. 3-12. XRD results for Cobalt oxide NPs synthesized at lower w/e ratio, 250°C, 20 MPa, 20 s. a. 0.8/0.2, b. 0.7/0.3, c. 0.5/0.5, d, peaklist of Co₃O₄.

化学式:	Co Co ₂ O ₄					
名称:	cobalt dicobalt(III) oxide				I/Ic (RIR値)= 4.45	
結晶系:	Cubic	空間群: Fd-3m(227)		実測密度:		
格子定数:	a=	8.0837	b=	8.0837	c=	8.0837
	α =	90.000	β =	90.000	γ =	90.000
	格子体積=	528.239	Z=	8	a	
参考文献:	Liu, X., Prewitt, C.T. Phys. Chem. Miner. 17(1990)168.					
線源:	CuK α 1	波長= 1.54060				
2 θ 範囲:	19.00 - 142.93					
コメント:	ANX: AB2X4. Analysis: Co ₃ O ₄ . Formula from original source: Co Co ₂ O ₄ . ICSD Collection Code: 69374. Temperature of Data Collection: 296 K. Wyckoff Sequence: e d a(FD3-MS). Unit Cell Data Source: Powder Diffraction.					

化学式:	Co Co ₂ O ₄					
名称:	cobalt dicobalt(III) oxide				I/Ic (RIR値)= 4.46	
結晶系:	Cubic	空間群: Fd-3m(227)		実測密度:		
格子定数:	a=	8.0968	b=	8.0968	c=	8.0968
	α =	90.000	β =	90.000	γ =	90.000
	格子体積=	530.811	Z=	8	b	
参考文献:	Liu, X., Prewitt, C.T. Phys. Chem. Miner. 17(1990)168.					
線源:	CuK α 1	波長= 1.54060				
2 θ 範囲:	18.97 - 142.38					
コメント:	ANX: AB2X4. Analysis: Co ₃ O ₄ . Formula from original source: Co Co ₂ O ₄ . ICSD Collection Code: 69366. Temperature of Data Collection: 580 K. Wyckoff Sequence: e d a(FD3-MS). Unit Cell Data Source: Powder Diffraction.					

化学式:	CO O					
名称:	COBALT OXIDE, PERICLASE				I/Ic (RIR値)= 4.93	
結晶系:		空間群: F m 3 m(225)		実測密度:		
格子定数:	a=	4.2630	b=	4.2630	c=	4.2630
	α =	90.000	β =	90.000	γ =	90.000
	格子体積=	77.472	Z=	4	c	
参考文献:						
線源:		波長=				
2 θ 範囲:	36.48 - 92.57					

Fig. 3-13. Lattice constant of cobalt oxide nanoparticles synthesized at a) 0.2, 0.3, 0.4 molar ratio of ethanol. b) 0.5 molar ratio of ethanol, c) 0.8 molar ratio of ethanol

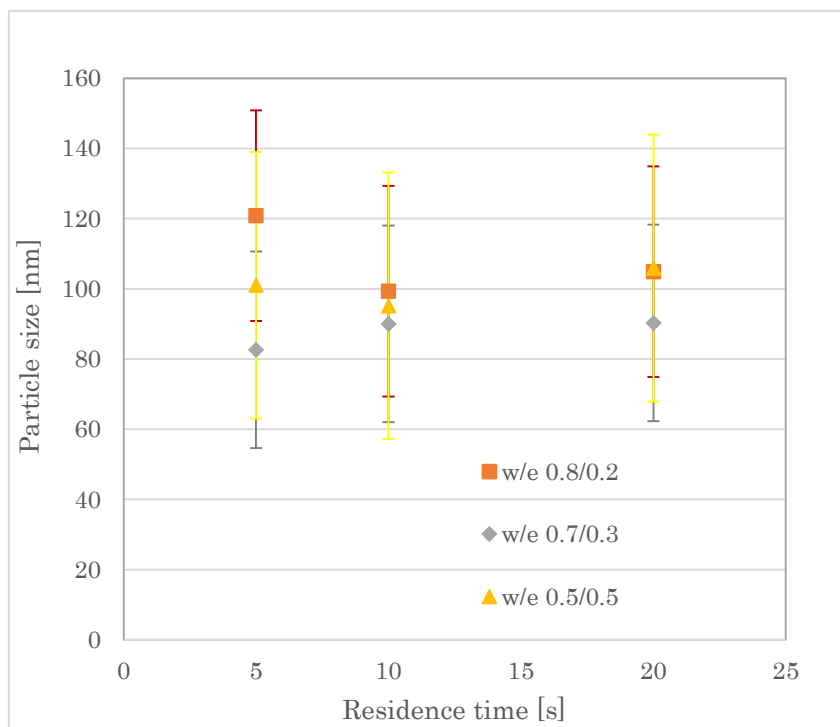


Fig. 3-14. Particle size of Cobalt oxide NPs synthesized at 0.8/0.2, 0.7/0.3, 0.5/0.5 w/e ratio, 5s, 10s, 20s reaction time.

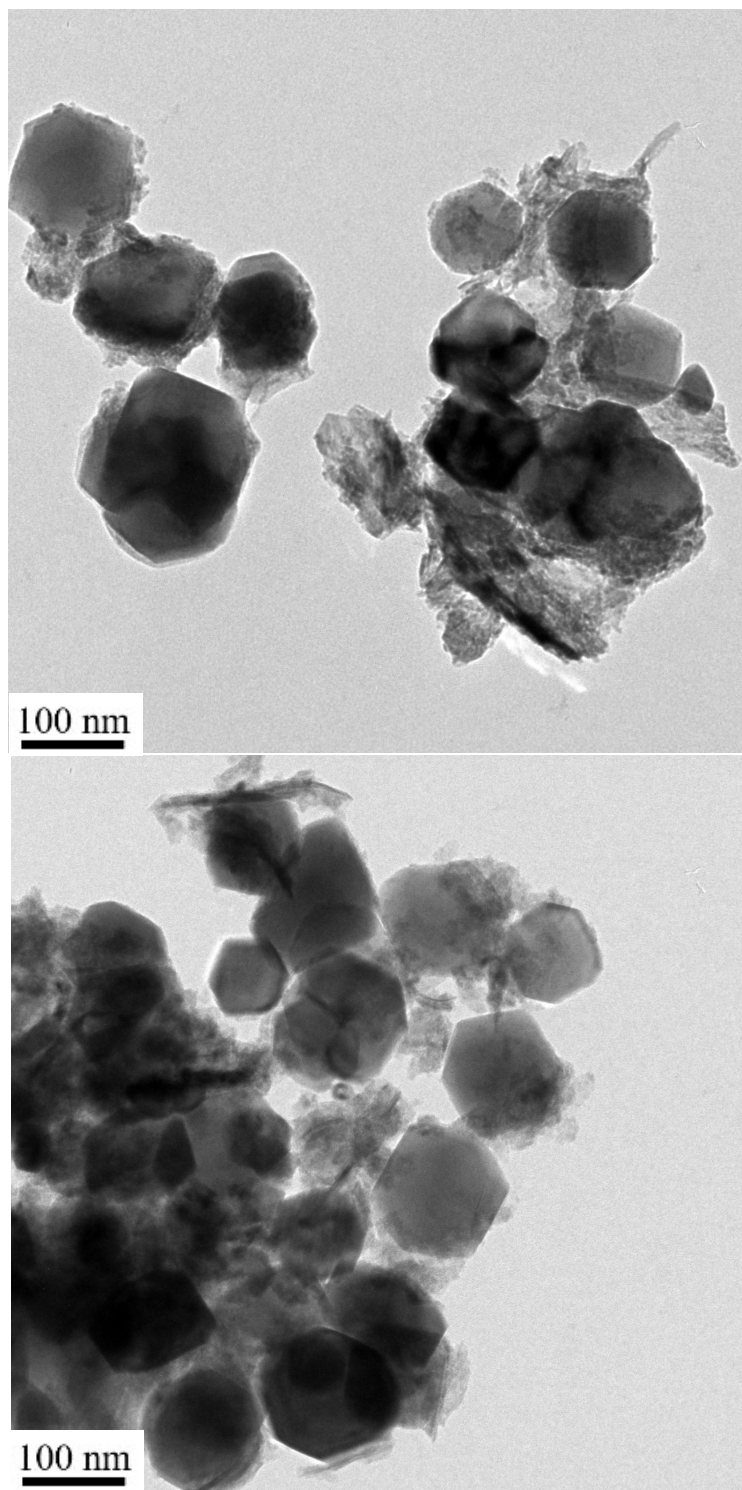


Fig. 3-15. Cobalt oxide nanoparticles synthesized at reaction time of 5 s, 0.5 molar ratio of ethanol.

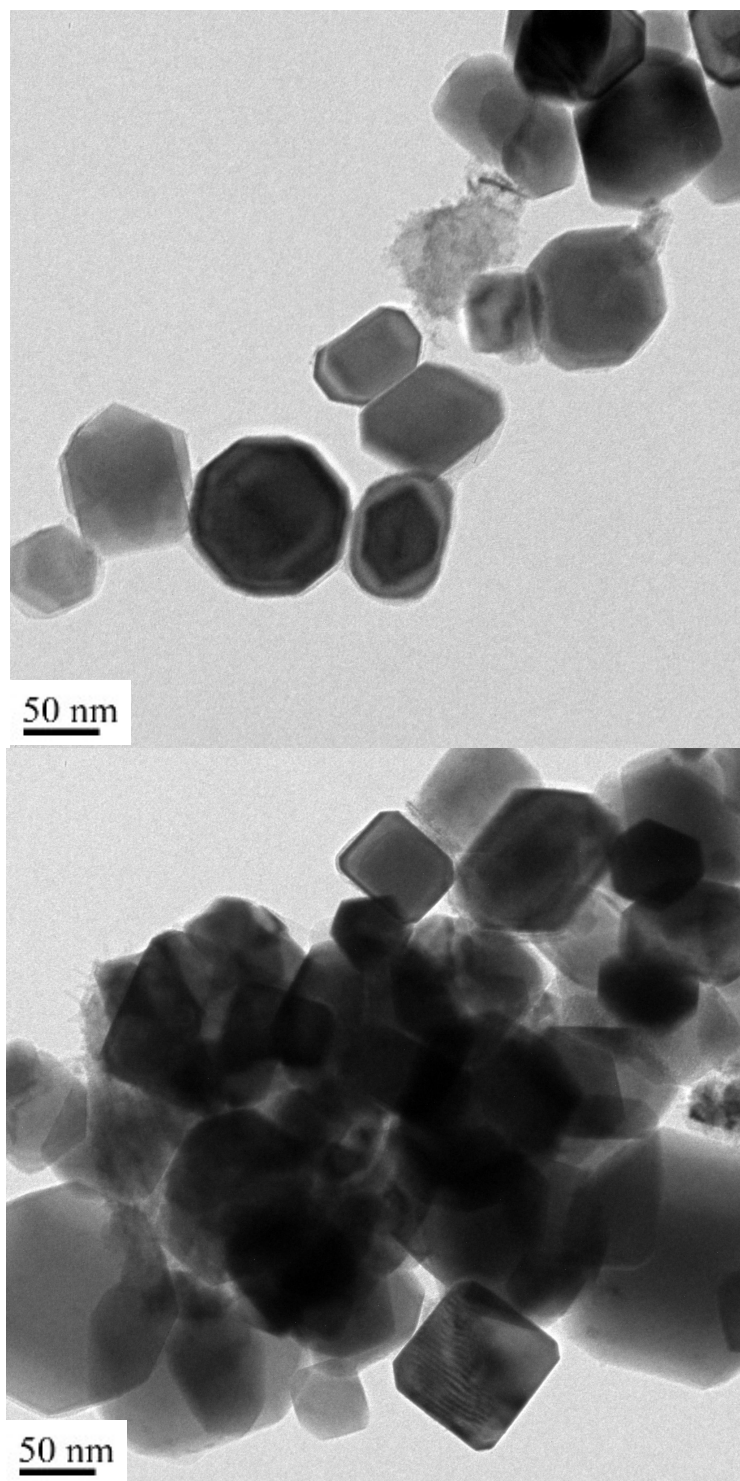


Fig. 3-16. Cobalt oxide nanoparticles synthesized at reaction time of 5 s, 0.5 molar ratio of ethanol.

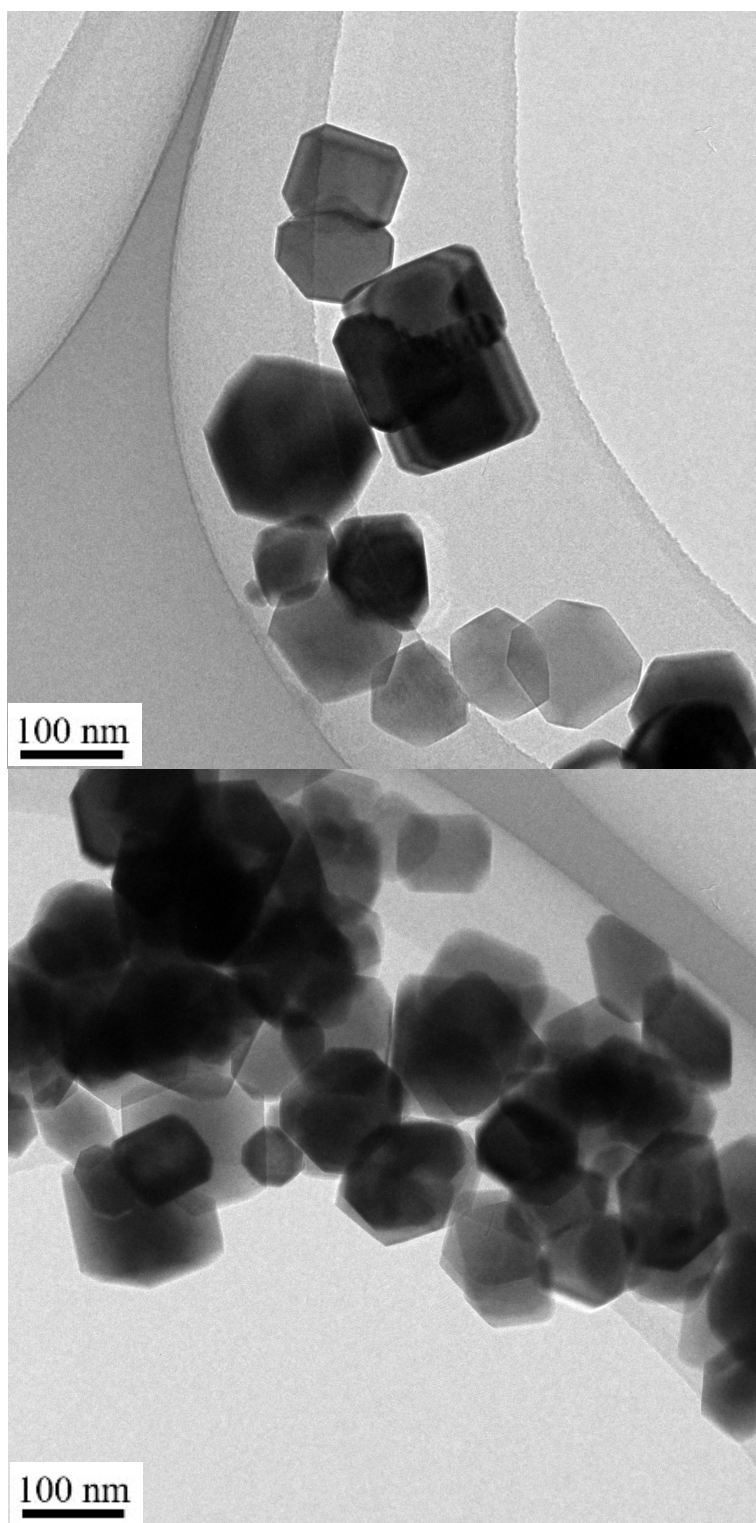


Fig. 3-17. Cobalt oxide nanoparticles synthesized at reaction time of 5 s, 0.5 molar ratio of ethanol.

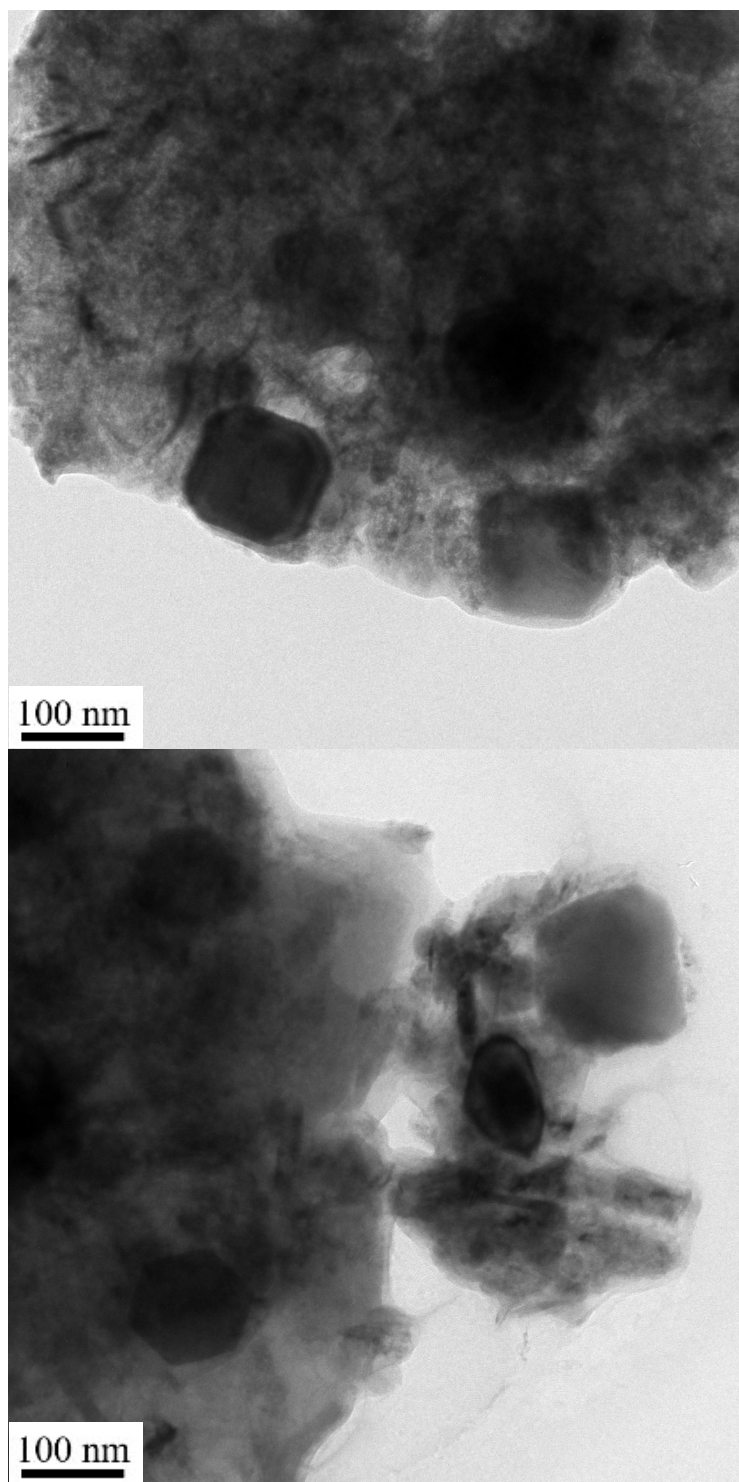


Fig. 3-18. Cobalt oxide nanoparticles synthesized at reaction time of 5 s, 0.6 molar ratio of ethanol.

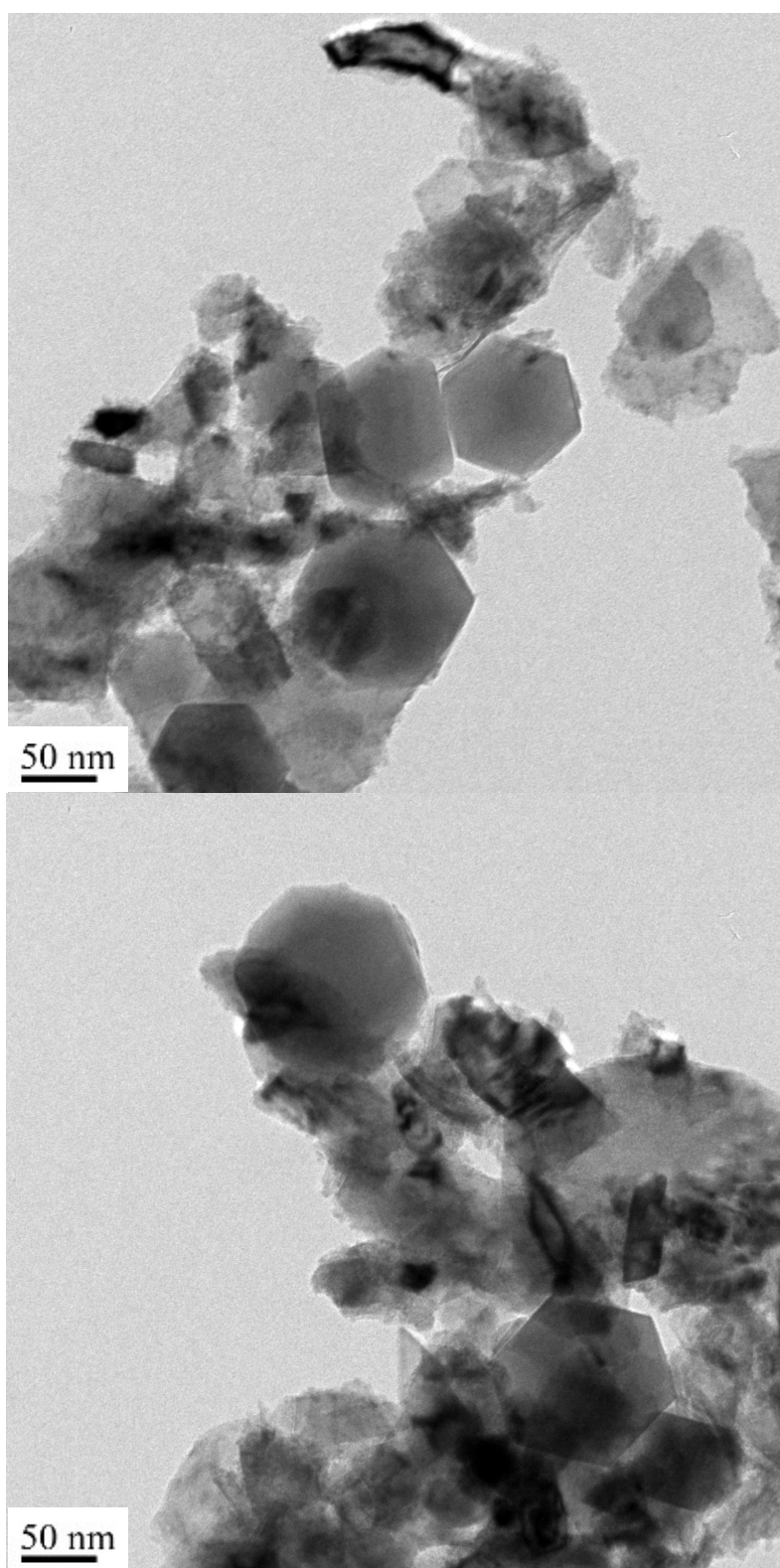


Fig. 3-19. Cobalt oxide nanoparticles synthesized at reaction time of 10 s, 0.6 molar ratio of ethanol.

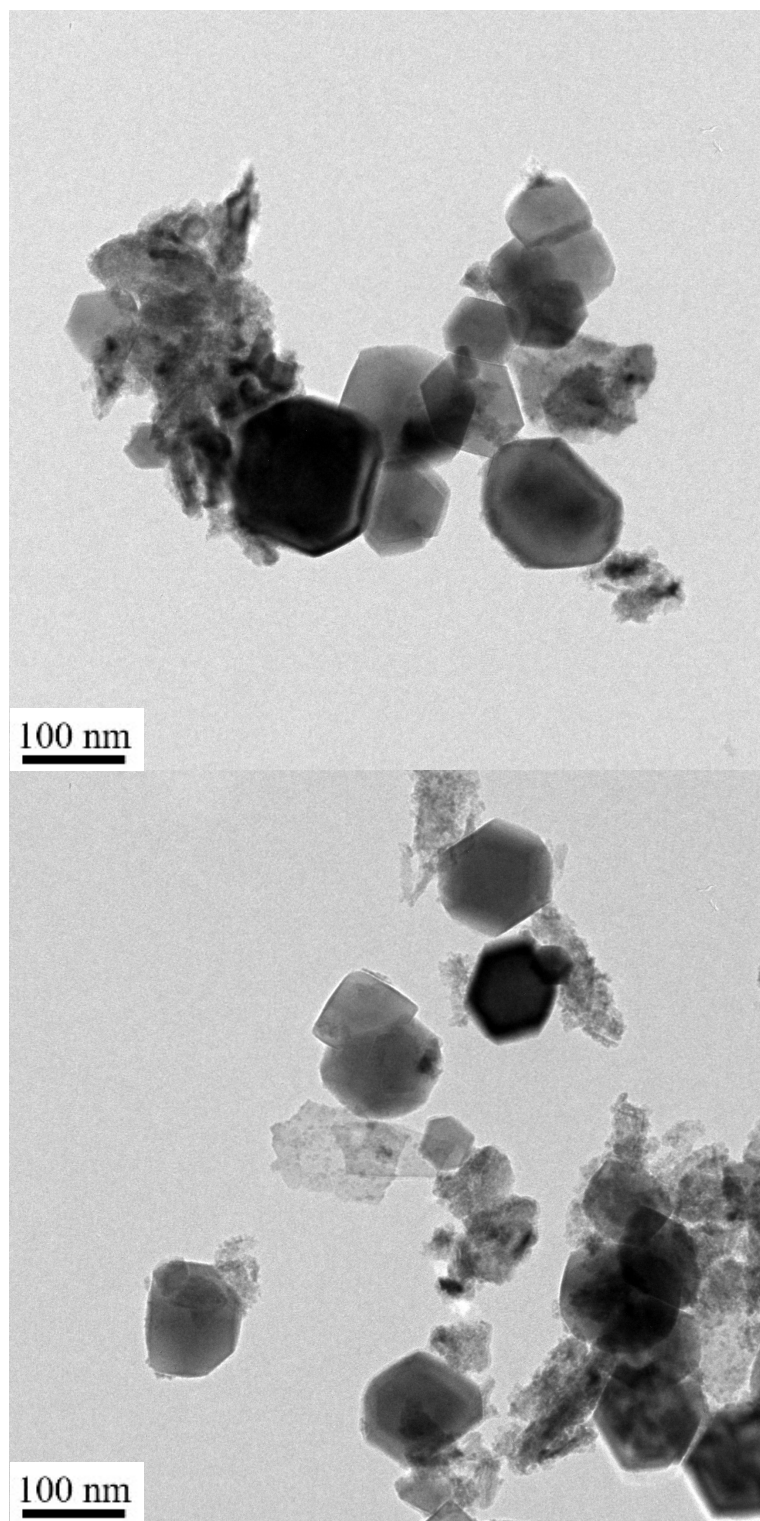


Fig. 3-20. Cobalt oxide nanoparticles synthesized at reaction time of 20 s, 0.6 molar ratio of ethanol.

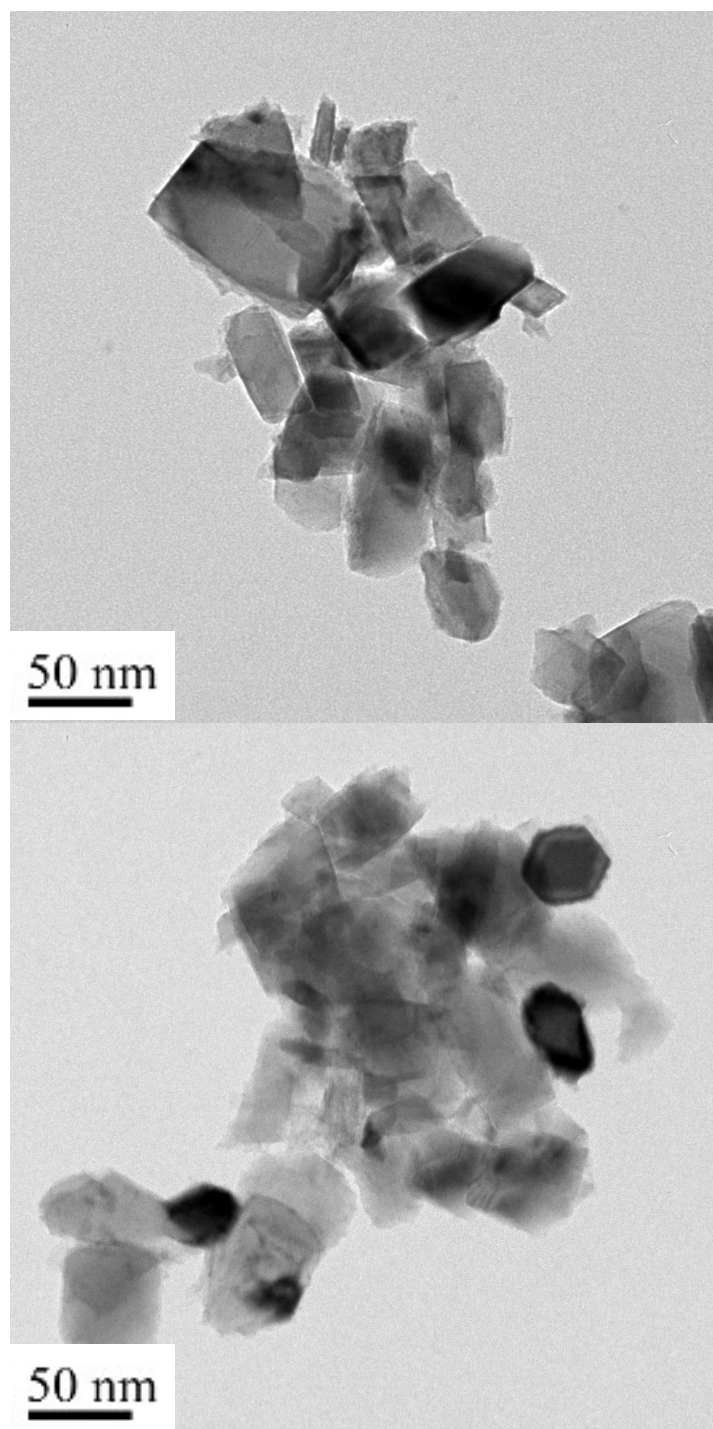


Fig. 3-21. Cobalt oxide nanoparticles synthesized at reaction time of 10 s, 0.8 molar ratio of ethanol.

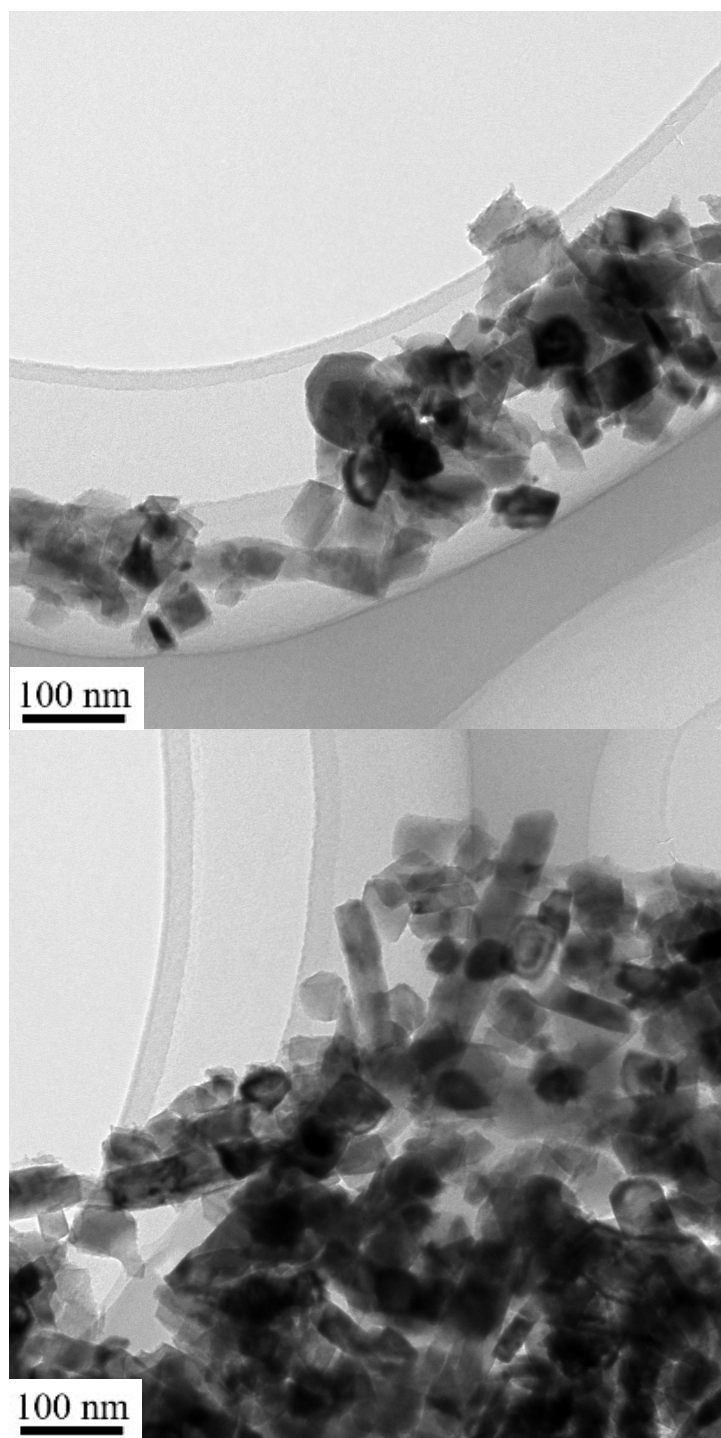


Fig. 3-22. Cobalt oxide nanoparticles synthesized at reaction time of 20 s, 0.8 molar ratio of ethanol.

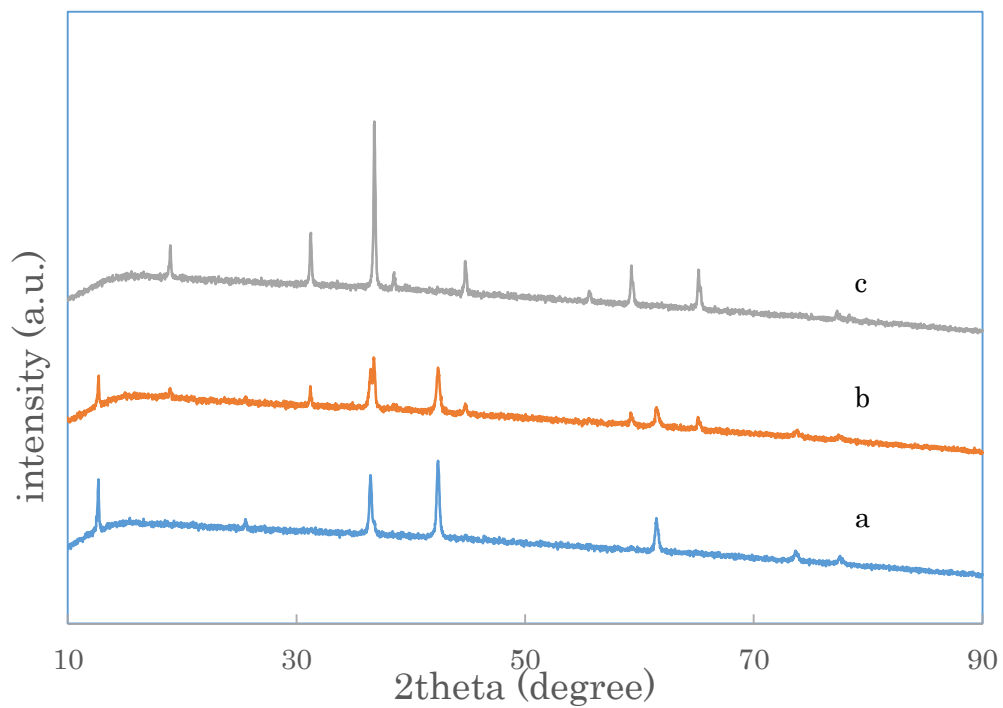


Fig. 3-23. XRD results for Cobalt oxide NPs synthesized at reaction time 10 s, 250°C, 20 MPa. a. 0.2/0.8, b. 0.4/0.6, c. 0.5/0.5. w/e ratio.

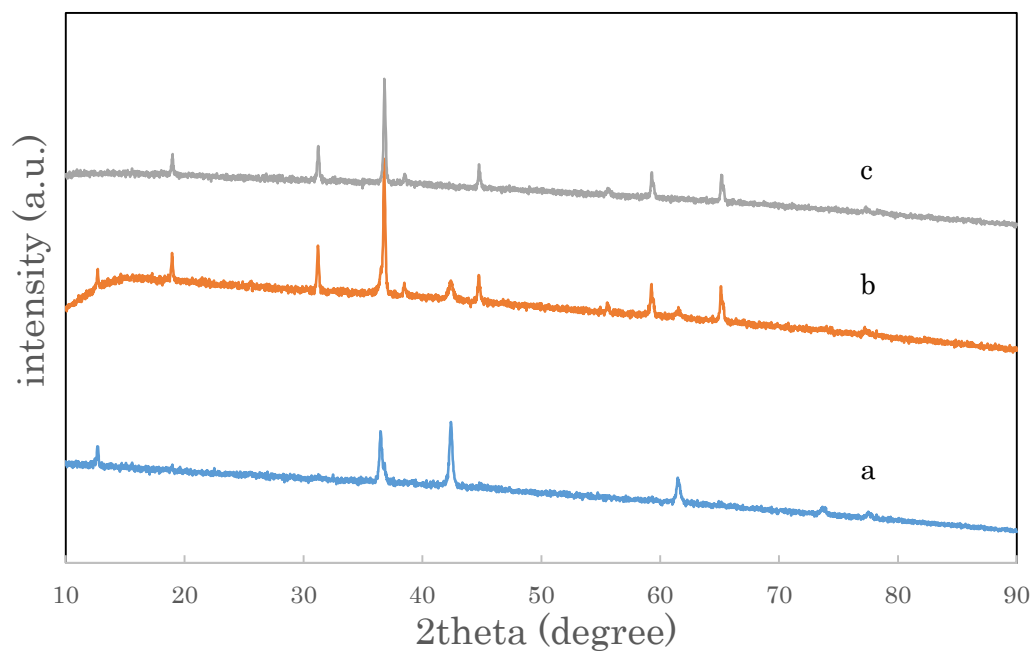


Fig. 3-24. XRD results for Cobalt oxide NPs synthesized at reaction time 20 s, 250°C, 20 MPa. a. 0.2/0.8, b. 0.4/0.6, c. 0.5/0.5. w/e ratio.

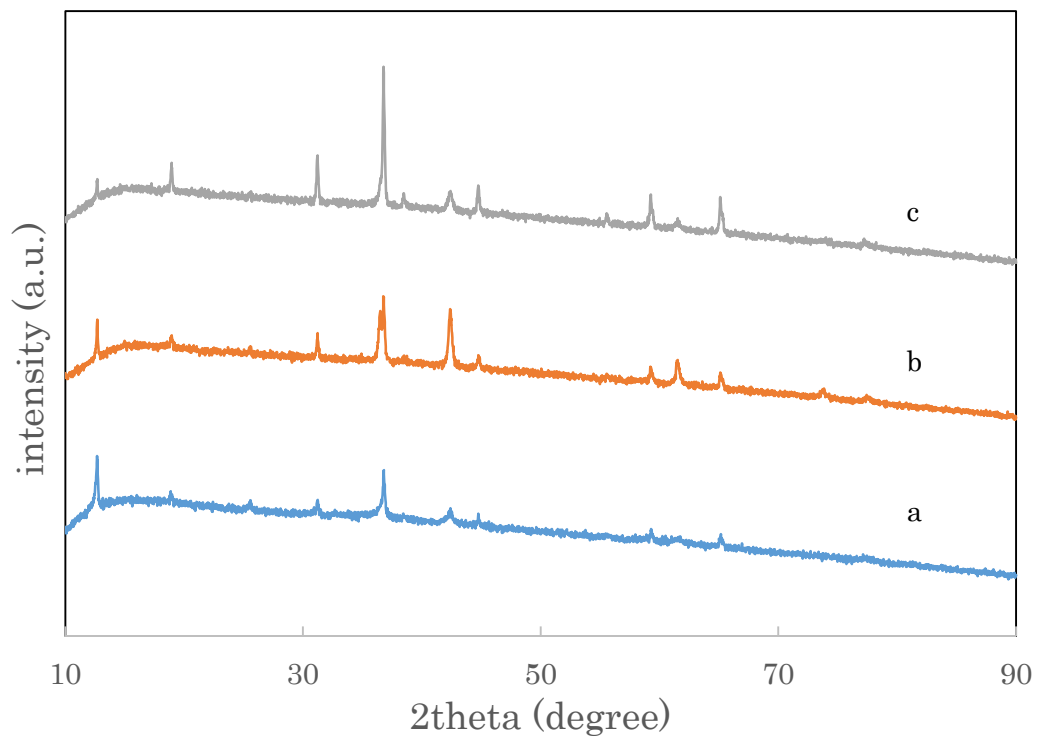


Fig. 3-25. XRD results for Cobalt oxide NPs synthesized at 0.4/0.6 w/e ratio, 250°C, 20 MPa. a. 5 s, b.10 s, c. 20 s.

Chapter 4 Conclusion

In this study, the syntheses of cobalt oxide NPs in a water-ethanol mixing solvent were conducted at 250°C 20 MPa from an ethanol molar ratio of 0 to 0.8 at different reaction times. The mixing of ethanol with water at a relatively low ratio and at a high temperature and high pressure caused lower solubility of cobalt ions. This resulted in a higher supersaturation of cobalt ions, thus enhancing the formation of nanoparticles. For similar reasons, as ethanol ratio increased from 0.2 to 0.3, the cobalt ions had a higher conversion and synthesized nanoparticles with smaller particle size. When the ethanol ratio was increased to 0.5, the reaction rate of NP synthesis and growth of (1 1 1) face of NPs became slower, which caused the shape of NPs to change from cubic to octagonal and round. When the ethanol ratio rose from 0.5 to 0.8, the redox potential of the mixed solvent changed and resulted in a more reductive environment for Co NPs synthesis. Conclusively, the composition of the nanoparticles was changed, and metal oxides with a lower valent number were synthesized.

And in the future research, to utilize this mixed solvent to realize the control of synthesis of metal oxide nanoparticles, three works need to be done. Firstly, calculation or experiment method need to be developed to evaluate the solubility of metal ions in water-ethanol mixed solvent at high temperature and high pressure condition. Secondly, the mechanism of how the ethanol reduces the higher valance number of metal to a lower valance also need to be studied. Finally, not only cobalt oxide nanoparticles, other metal species also need be tried in such a system.

Reference

- [1] Bødker et al., "Surface effects in metallic iron nanoparticles," *Physical Review Letters*, 1994.
- [2] Paul Alivisatos et al., "Perspectives on the physical chemistry of semiconductor nanocrystals," *The Journal of Physical Chemistry*, 1996.
- [3] 厚生労働省., "ナノマテリアルの安全対策に関する検討会報告書,"
- [4] 粉体工学会編, 粉体工学業書 第2巻 "粉体の生成," 日刊工業新聞., 2005.
- [5] Mitsuo Uematsu et al., "Static Dielectric Constant of Water and Steam," *Journal of Physical and Chemical Reference Data*, 1980.
- [6] M Born., "Free energy of solvation," *Z. Phys.*, 1920.
- [7] Tadafumi Adschiri et al., "Kinetics and mechanism of cellobiose hydrolysis and retro-aldol condensation in subcritical and supercritical water," *Industrial & Engineering Chemistry Research*, 2002.
- [8] Shin-Ichiro Kawasaki et al., "Engineering study of continuous supercritical hydrothermal method using a T-shaped mixer: Experimental synthesis of NiO nanoparticles and CFD simulation," *The Journal of Supercritical Fluids*, 2010.
- [9] T.J. Bruno, J.F. Ely, *Supercritical Fluids Technology: Reviews in Modern Theory and Applications*, CRC Press, Boca Raton, FL, 1991.
- [10] M.A. McHugh, V.J. Krukonis, *Supercritical Fluid Extraction: Principles and Practice*, Butterworth-Heinemann, Boston, 1994.
- [11] P.E. Savage, *Chem. Rev.* 99 (1999) 603–621.
- [12] J.D. Holmes, K.P. Johnston, R.C. Doty, B.A. Korgel, *Science* 287 (2000) 1471–1473. [13] M.A. Frisch, L. Li, E.F. Gloyna, in: *Proceedings of the 49th Industrial Waste Conference*, Lewis Publishers, West Lafayette, IN, 1994, p. 353.
- [14] P.G. Jessop, Y. Hsiao, T. Ikariya, R. Royori, *J. Am. Chem. Soc.* 118 (1996) 344–355. [15] A.K. Dillow, K.P. Hafner, S.L.J. Yun, F. Deng, S.G. Kazarian, C.L. Liotta, C.A. Eckert, *AIChE J.* 43 (1997) 515–524.
- [16] R.B. Gupta, J.R. Combes, K.P. Johnston, *J. Phys. Chem.* 97 (1993) 707–715.
- [17] J.B. Ellington, K.M. Park, J.F. Brennecke, *Ind. Eng. Chem. Res.* 33 (1994) 965–974.
- [18] J.S. Brown, H.P. Lesutis, D.R. Lamb, D. Bush, K. Chandler, B.L. West, C.L. Liotta, C.A. Eckert, D. Schiraldi, J.S. Hurley, *Ind. Eng. Chem. Res.* 38 (1999) 3622–3627.
- [19] D. Andrew, B.T. Des Islet, A. Margaritis, W.A.C., *J. Am. Chem. Soc.* 117 (1995) 6132–6133.
- [20] C. Habenicht, L.C. Kam, M.J. Wilschut, M.J. Antal Jr., *Ind. Eng. Chem. Res.* 34 (1995) 3784–3792.
- [21] J. Walendziewski, J. Trawczynski, *Ind. Eng. Chem. Res.* 35 (1996) 3356–3361.
- [22] L. Bagnell, C.R. Strauss, *Chem. Commun.* (1999) 287–288.
- [23] O. Kajimoto, *Chem. Rev.* 99 (1999) 355–389.

- [24] S.C. Tucker, *Chem. Rev* 99 (1999) 391–418.
- [25] J.F. Brennecke, J.E. Chateauf, *Chem. Rev.* 99 (1999) 433–452.
- [26] M.E. Sigman, S. Lindley, J.E. Leffler, *J. Am. Chem. Soc.* 107 (1985) 1471–1472.
- [27] J.A. Hyatt, *J. Org. Chem.* 49 (1984) 5097–5101.
- [28] C.R. Yonker, S.L. Frye, D.R. Kalkwarf, R.D. Smith, *J. Phys. Chem.* 90 (1986) 3022–3026.
- [29] Y.-P. Sun, M.A. Fox, K.P. Johnston, *J. Am. Chem. Soc.* 114 (1992) 1187–1194.
- [30] S. Gupta, V. Kumar, K.B. Joshi, Solvent mediated photo-induced morphological transformation of AgNPs-peptide hybrids in water-EtOH binary solvent mixture, *J. Mol. Liq.* 236 (2017) 266e277.
- [31] C.S. Biswas, E. Sulu, B. Hazer, Effect of the composition of methanol-water mixtures on tacticity of poly(N-ethylacrylamide) gel, *J. Appl. Polym. Sci.* 132 (2015) 41668.
- [32] R.Y. Li, C. D'Agostino, J. McGregor, M.D. Mantle, J.A. Zeitler, L.F. Gladden, Mesoscopic structuring and dynamics of alcohol/water solutions probed by terahertz time-domain spectroscopy and pulsed field gradient nuclear magnetic resonance, *J. Phys. Chem. B* 118 (2014) 10156e10166.
- [33] A. Perera, F. Sokolic, L. Almasy, Y. Koga, Kirkwood-Buff integrals of aqueous alcohol binary mixtures, *J. Chem. Phys.* 124 (2006) 124515.
- [34] H.A. Zarei, N. Mirhidari, Z. Zangeneh, Densities, excess molar volumes, viscosity, and refractive indices of binary and ternary liquid mixtures of methanol (1) þ ethanol (2) þ 1,2-propanediol (3) at P¼81.5 kPa, *J. Chem. Eng. Data* 54 (2009) 847e854.
- [35] R.J. Sengwa, S. Sankhla, N. Shinyashiki, Dielectric parameters and hydrogen bond interaction study of binary alcohol mixtures, *J. Solut. Chem.* 37 (2008) 137e153.
- [36] J. Safarov, S. Heydarov, A. Shahverdiyev, E. Hassel, Excess molar volumes $V_m(E)$, isothermal compressibilities k , and thermal expansivities α of $\{(1-x)H_2O \text{ þ } xCH_3OH\}$ at $T \text{ (} 298.15 \text{ to } 523.15 \text{ K)}$ and pressures up to 60 MPa, *J. Chem. Thermodyn.* 36 (2004) 541e547.
- [37] M. Nedic, T.N. Wassermann, R.W. Larsen, M.A. Suhm, A combined Raman- and infrared jet study of mixed methanol-water and ethanol-water clusters, *PCCP* 13 (2011) 14050e14063.
- [38] I. Juurinen, K. Nakahara, N. Ando, T. Nishiumi, H. Seta, N. Yoshida, T. Morinaga, M. Itou, T. Ninomiya, Y. Sakurai, E. Salonen, K. Nordlund, K. Hamalainen, M. Hakala, Measurement of two solvation regimes in water-ethanol mixtures using x-ray compton scattering, *Phys. Rev. Lett.* 107 (2011) 197401.
- [39] T. Pradhan, P. Ghoshal, R. Biswas, Structural transition in alcohol-water binary mixtures: a spectroscopic study, *J. Chem. Sci.* 120 (2008) 275e287.
- [40] M. Kiselev, S. Noskov, Y. Puthovski, T. Kerdcharoen, S. Hannongbua, The study of hydrophobic hydration in supercritical water-methanol mixtures, *J. Mol. Graph. Model.* 19 (2001) 412e416.
- [41] M.L. Tan, B.T. Miller, J. Te, J.R. Cendagorta, B.R. Brooks, T. Ichiye, Hydrophobic hydration and the anomalous partial molar volumes in ethanol-water mixtures, *J. Chem. Phys.* 142 (2015) 064501.

- [42] J.C. Soetens, P.A. Bopp, Water-methanol mixtures: simulations of mixing properties over the entire range of mole fractions, *J. Phys. Chem. B* 119 (2015) 8593e8599.
- [43] S.P. Benson, J. Pleiss, Incomplete mixing versus clathrate-like structures: a molecular view on hydrophobicity in methanol-water mixtures, *J. Mol. Model.* 19 (2013) 3427e3436.
- [44] A. Perera, L. Zoranic, F. Sokolic, R. Mazighi, A comparative Molecular Dynamics study of water-methanol and acetone-methanol mixtures, *J. Mol. Liq.* 159 (2011) 52e59.
- [45] M.M. Hoffmann, M.S. Conradi, Are there hydrogen bonds in supercritical water? *J. Am. Chem. Soc.* 119 (1997) 3811-3817
- [46] Sue, K., et al (2011). *Chemical Engineering Journal*, 166(3), 947–953.
- [47] Slostowski, C., et al (2012). *Langmuir*, 28(48), 16656–16663.
- [48] Mi, J. L., et al (2014). *Journal of Physical Chemistry C*, 118(20), 11104–11110.
- [49] Reverón, H., et al (2005). *Nanotechnology*, 16(8), 1137–1143.
- [50] Cabañas, A., et al (2007). *The Journal of Supercritical Fluids*, 40(2), 284–292.
- [51] Yoko. et al. Nano-size control of BaTiO₃ particles using supercritical water-ethanol mixed solvent (2018) SCEJ 50th autumn meeting
- [52] Sugimoto, T. *Monodispersed Particles*; Elsevier: Amsterdam, 2001
- [53] Rogach, A.; Talapin, D.; Shevchenko, E.; Kornowski, A.; Haase, M.; Weller, H. *Adv. Funct. Mater.* 2002, 12, 653.
- [54] Ono, T. et al. Measurement and correlation of density and viscosity of n-alcohol–water mixtures at temperatures up to 618 K and at pressures up to 40 MPa. *Fluid Phase Equilib.* 453, 13–23 (2017).
- [55] Kwon, S. G.; Hyeon, T. *Small*. 2011, 7, 2685

Acknowledgments

Firstly, I really appreciate all the people who helped me at the process of my research, especially professor Oshima, as the supervisor of my thesis, he taught me how to find the topic that I am really interested in and what can be called a research. And also Lecturer Akizuki, who really gave me lots of supports with patience and kindness during all the two year and a half research life. Lecturer Masanori Aichi provided advice on research. I am very grateful to him. Assistant Professor Ken Yajima of the X-ray Measurement Room of the Institute for Solid State Physics, and Daisuke Hamane of the Electron Microscope Room also taught me a lot about the way to use XRD and TEM. And very grateful to Assistant Professor Matsuo for helping me to use the UV-Vis. Of course, very appreciate to Dr. Orita for teaching me how to do the experiments and how to push my research step by step.

And thanks to all the members in Oshima, Otomo, and Akizuki lab for giving me an enriched and enjoying school life. Especially my brother Mr. Liao, Mr. Ma, and Mr. Feng, who gave me good companion during the lonely days. And, all the cute younger generations in our lab, I am very grateful to having you guys at the last half years in school.